Hydrodynamic processes in sharp meander bends and their morphological implications

K. Blanckaert[1,2,3]

Received 1 July 2010; revised 24 October 2010; accepted 3 November 2010; published 29 January 2011.

[1] The migration rate of sharp meander bends exhibits large variance and indicates that some sharply curved bends tend to stabilize. These observations remain unexplained. This paper examines three hydrodynamic processes in sharp bends with fixed banks and discusses their morphological implications: secondary flow saturation, outer-banks cells, and inner-bank flow separation. Predictions from a reduced-order hydrodynamic model show that nonlinear hydrodynamic interactions limit the growth of the secondary flow. This process is called the saturation of the secondary flow. For outer-bank cells and inner-bank flow separation, the analysis relies on experimental findings from flume studies in channels with fixed and mobile beds. The experiments reveal that outer-bank cells exist near steep as well as shelving banks and amplify with increasing steepness and roughness of the outer bank, and especially with increasing curvature. The effects of flow separation at the inner bank are found to be strongly conditioned by flow-sediment interactions, which lead to an increased scour depth near the outer bank and increased velocities near the toe of that bank. Overall the results suggest that secondary flow saturation and outer-bank cells tend to inhibit meander migration, whereas inner-bank separation may enhance migration. The relative importance of these three hydrodynamic processes depends on hydraulic, geometric, and sedimentologic conditions, which is consistent with the large variance in observed migration rates. The results suggest that large shallow rivers have the most dynamic meandering behavior, while the occurrence of stabilized meanders seems to be favored in narrow rivers.

Citation: Blanckaert, K. (2011), Hydrodynamic processes in sharp meander bends and their morphological implications, *J. Geophys. Res.*, *116*, F01003, doi:10.1029/2010JF001806.

1. Introduction

[2] Lowland rivers seldom follow a straight course but typically meander in their alluvial plain. Meander migration through bank erosion and accretion results in reworking of the floodplain and valley widening. Meandering is the result of an intricate interaction of hydrological, hydrodynamical, geomorphological and ecological processes. Apart from being scientifically interesting, meander migration is of great practical importance.

[3] Although a considerable amount of research has been conducted on meandering rivers, understanding of the dynamics of meandering is still incomplete, in particular with respect to how these dynamics are controlled by variations in channel and planform characteristics. Past work has indicated that the hydrodynamics of sharp bends may differ from those for bends with moderate or mild curvature [e.g., *Bagnold*, 1960; *Leeder and Bridges*, 1975; *Hickin*, 1977, 1978; *Nanson*, 2010]. The purpose of this paper is to examine three hydrodynamical processes in sharp bends and to explore their implications for meander migration: (1) curvature-induced secondary flow, which is a characteristic feature of curved-open channel flow; (2) additional outer-bank cells of secondary flow; and (3) horizontal flow recirculation at the (convex) inner bank. Figure 1 conceptually illustrates these three hydrodynamic processes.

[4] Mathematical models for meander migration are able to reproduce large-scale and long-term processes such as the growth and migration of meander bends, the asymmetrical meander shape, the formation of multilobed meander bends and the scale invariance of the meandering process. Although these simulated processes look remarkably realistic, they lack validation by means of field observations. Despite the rapid evolution in computational power, prediction of long-term and large-scale meander processes is only feasible by means of reduced-order models, which limit the computational cost by means of simplified and parameterized descriptions of the flow and the bank erosion processes. The description of the

[1]State Key Laboratory of Urban and Regional Ecology, Research Center for Eco-Environmental Sciences, Chinese Academy of Sciences, Beijing, China.
[2]Laboratory of Hydraulic Constructions, School of Architecture, Civil and Environment Engineering, École Polytechnique Fédérale Lausanne, Lausanne, Switzerland.
[3]Faculty of Civil Engineering and Geosciences, Delft University of Technology, Delft, Netherlands.

0148-0227/11/2010JF001806

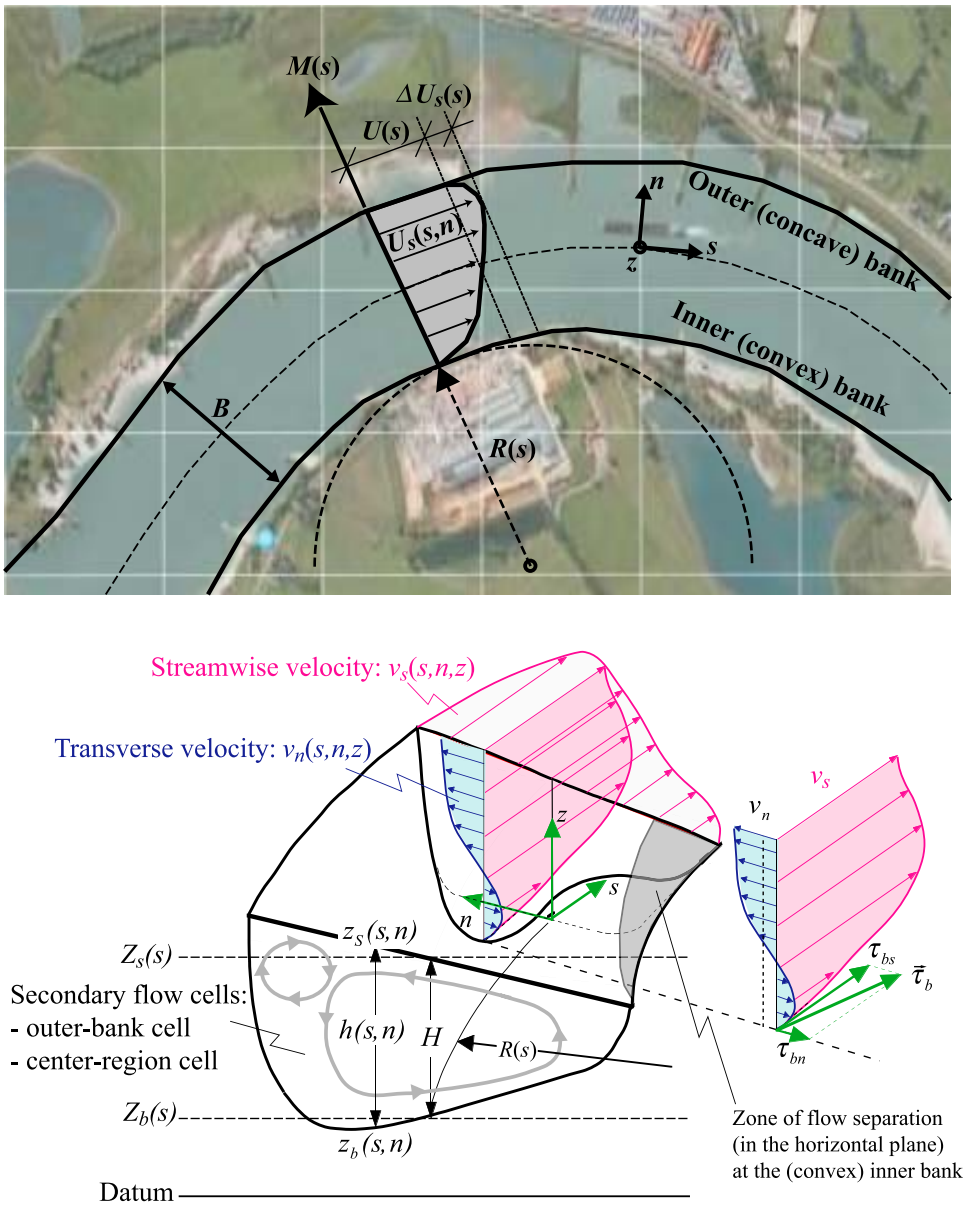

Figure 1. Conceptual sketch of the relevant processes in meander bends and definition sketch of the reference system and the most relevant variables.

flow is mostly based on the depth-averaged flow equations supplemented by a parameterization of three-dimensional flow effects (Figure 1), whereas the bank erosion is modeled as driven by the meander hydrodynamics. Henceforward only reduced-order models will be considered; a more general discussion of meander models is reported by *Blanckaert and de Vriend* [2010]. Such reduced-order models have been progressively developed and refined during the last decades [e.g., *Ikeda et al.*, 1981; *Parker et al.*, 1982, 1983; *Howard*, 1984; *Blondeaux and Seminara*, 1985; *Parker and Andrews*, 1986; *Odgaard*, 1986; *Furbish*, 1988; *Seminara and Tubino*, 1992; *Liverpool and Edwards*, 1995; *Stølum*, 1996, 1998; *Imran et al.*, 1999; *Edwards and Smith*, 2002; *Lancaster and Bras*, 2002; *Camporeale et al.*, 2007; *Crosato*, 2008; *Bolla Pittaluga et al.*, 2009]. Comprehensive summaries and comparisons of these reduced-order meander models are reported by *Camporeale et al.* [2007] and *Crosato* [2008, chap. 4]. *Blanckaert and de Vriend* [2010] review and compare the most recent reduced-order hydrodynamic models [*Odgaard*, 1989; *Johannesson and Parker*, 1989a; *Imran et al.*, 1999; *Zolezzi and Seminara*, 2001; *Bolla Pittaluga et al.*, 2009].

[5] Because meanders are characterized by a constant width, B, at least from a statistical and long-term point of view, the rates of accretion at the (convex) inner bank and erosion at the (concave) outer bank, M, are assumed to be equal and to be proportional to the excess of velocity at the bank, ΔU_s, with respect to the cross-sectional averaged velocity, U:

$$M \sim \Delta U_s \tag{1}$$

Figure 1 illustrates this relation and defines the width B, the radius of curvature at the centerline R, the reference system

(s, n, z), the corresponding velocity components (v_s, v_n, v_z), their depth-averaged values (U_s, U_n), the bed shear stress components (τ_{bs}, τ_{bn}), and the local bed level z_b, water surface level z_S and flow depth h as well as their cross-sectional averaged values, Z_b, Z_S and H, respectively. Although this simple parameterization of the bank migration seems to be justified by field observations [*Pizzuto and Meckelnburg*, 1989], it does not account for the complex near-bank hydrodynamics, such as the outer-bank cell of secondary flow (Figure 1) [e.g., *Hey and Thorne*, 1975; *Bridge and Jarvis*, 1977; *Bathurst et al.*, 1977, 1979; *Thorne and Hey*, 1979; *Dietrich and Smith*, 1983; *de Vriend and Geldof*, 1983; *Thorne et al.*, 1985; *Markham and Thorne*, 1992], and flow separation at the (convex) inner (Figure 1) [*Leeder and Bridges*, 1975; *Frothingham and Rhoads*, 2003; *Ferguson et al.*, 2003] or (concave) outer bank [*Hickin*, 1977; *Jackson*, 1992; *Andrle*, 1994; *Hodskinson and Ferguson*, 1998], which are often observed in open-channel bends and may be relevant for meander migration.

[6] In reduced-order meander models, the secondary flow (Figure 1) is a main driving force of the velocity excess. This secondary flow is related to the river planform and can primarily be expressed as a convolution function of the channel curvature [*Güneralp and Rhoads*, 2009]. This secondary flow induces a transverse component of the bed shear stress τ_{bn} (Figure 1), which conditions the development of a transverse bed slope with increasing flow depth in outward direction [*Olesen*, 1987; *Camporeale et al.*, 2007]. Moreover, it redistributes momentum, causing velocities to increase toward the outer bank, which in turn leads to differential sediment transport over the width that amplifies the development of the transverse bed slope.

[7] Reduced-order models predict a cyclic dynamic state: meanders keep migrating and expanding until the upstream and downstream limbs of a bend meet, which cuts off an oxbow lake, restraightens the river locally, and initiates a new meander growth cycle. Although cutoffs and the formation of oxbow lakes are prominent features of meandering streams, this predicted evolution does not fully agree with field observations.

[8] Figure 2 summarizes field observations on the meander migration rate by *Hickin* [1974, 1978], *Hickin and Nanson* [1975, 1984], *Nanson and Hickin* [1983, 1986], *Hooke* [1987], *Biedenharn et al.* [1989], *Hudson and Kesel* [2000], and *de Kramer et al.* [2000]. Since *Hickin* [1974] and *Hickin and Nanson* [1975] recognized that meander curvature exerts the dominant control on meander migration, the migration rate M has systematically been investigated and represented as a function of the dimensionless curvature B/R (Figure 2). Based on measurements on the Beatton River (Figure 2b) [*Hickin and Nanson*, 1975, 1984], *Hickin* [1974, 1977] developed a conceptual model of meander migration involving initiation, growth and termination stages (Figure 2a): the meander migration rate increases in the initial stage of meandering, accelerates in the so-called growth period of meandering, reaches a maximum migration rate and ultimately slows down in sharp meander bends. In the present paper, the initiation, growth, and termination stages of meanders correspond to the notions of mildly, moderately, and sharply curved bends, respectively (Figure 2). According to this simplified parameterization of the degree of curvature, open-channel bends are sharply curved when the curvature ratio B/R is larger than a value of about 0.5 (or $R/B < 2$). This meander behavior according to *Hickin*'s [1974, 1977] conceptual model was confirmed by data from 21 rivers in western Canada (Figure 2c) [*Hickin and Nanson*, 1984] as well as by data from the Allier River and the Border Meuse (Figures 2d and 2e, respectively) [*de Kramer et al.*, 2000]. These field observations even suggest that meanders may reach an ultimate state of equilibrium whereby any lateral migration is arrested and no cutoffs occur. Data on the River Dane (Figure 2f) [*Hooke*, 1987] and the Mississippi River (Figure 2g) [*Hudson and Kesel*, 2000], on the contrary, do not show any clear trend in tight bends and are characterized by a large variance in migration rates.

[9] Obviously, the migration rate of meanders depends on multiple parameters, including the meander planform (which defines the evolution of the centerline radius of curvature R, the width B and the influences of upstream and downstream bends), the average flow depth H, the sediment characteristics, the bank erodibility and the roughness. The latter will be parameterized by the dimensionless Chézy coefficient $C_f = gR_hE_s/U^2$ based on the hydraulic radius R_h and the energy gradient E_s. Recent work on the trajectories of individual bends [*Hooke*, 2003; *Güneralp and Rhoads*, 2010] shows they are complex. The restriction to the single influence of the curvature ratio B/R unavoidably leads to important scatter in Figure 2. Nevertheless, Figure 2 clearly reveals that sharply curved bends exhibit large variance in migration rates and that some sharply curved bends are characterized by a reduction in migration rates. *Hooke* [2003] attempted to account for both observations in her extension of Hickin's conceptual model, by proposing four different types of meandering behavior, summarized in Figure 2a: types "A" and "B" are so-called active meanders that periodically reach cutoff, type "C" represents streamwise migrating meanders without cutoff events and type "D" represents stabilized meanders. Existing reduced-order meander models are neither able to predict the reduced migration rate in sharp bends, nor the large observed variance in migration rates, presumably because essential hydrodynamic and/or morphodynamic processes are not accounted for in these models.

[10] This observed behavior of sharp meander bends and its relation to hydrodynamic and/or morphodynamic processes has been amply discussed in the literature. Table 1 summarizes suggested causes for the apparent maximum migration rate and the reduced migration rate in sharp bends (Figure 2a). According to *Furbish* [1988], however, the maximum migration rate at an intermediate curvature ratio is only apparent, because a monotonic increase is obtained when considering reach-averaged values to characterize the meander bends. This controversy on the behavior of sharp meander bends further confirms that the processes underlying the different types of meandering, the large variance in migration rates, and the reduced migration rate in some sharp bends, as well as their dependence on geometric, hydraulic and sedimentologic parameters are still poorly understood. Sections 3, 4, and 5 investigate three hydrodynamic processes that are not accounted for in existing reduced-order meander models and discuss their morphological implications.

[11] 1. Reduced-order hydrodynamic models [e.g., *van Bendegom*, 1947; *Rozovskii*, 1957; *Engelund*, 1974; *de Vriend*, 1977; *Johannesson and Parker*, 1989a; *Imran et al.*, 1999; *Zolezzi and Seminara*, 2001; *Bolla Pittaluga*

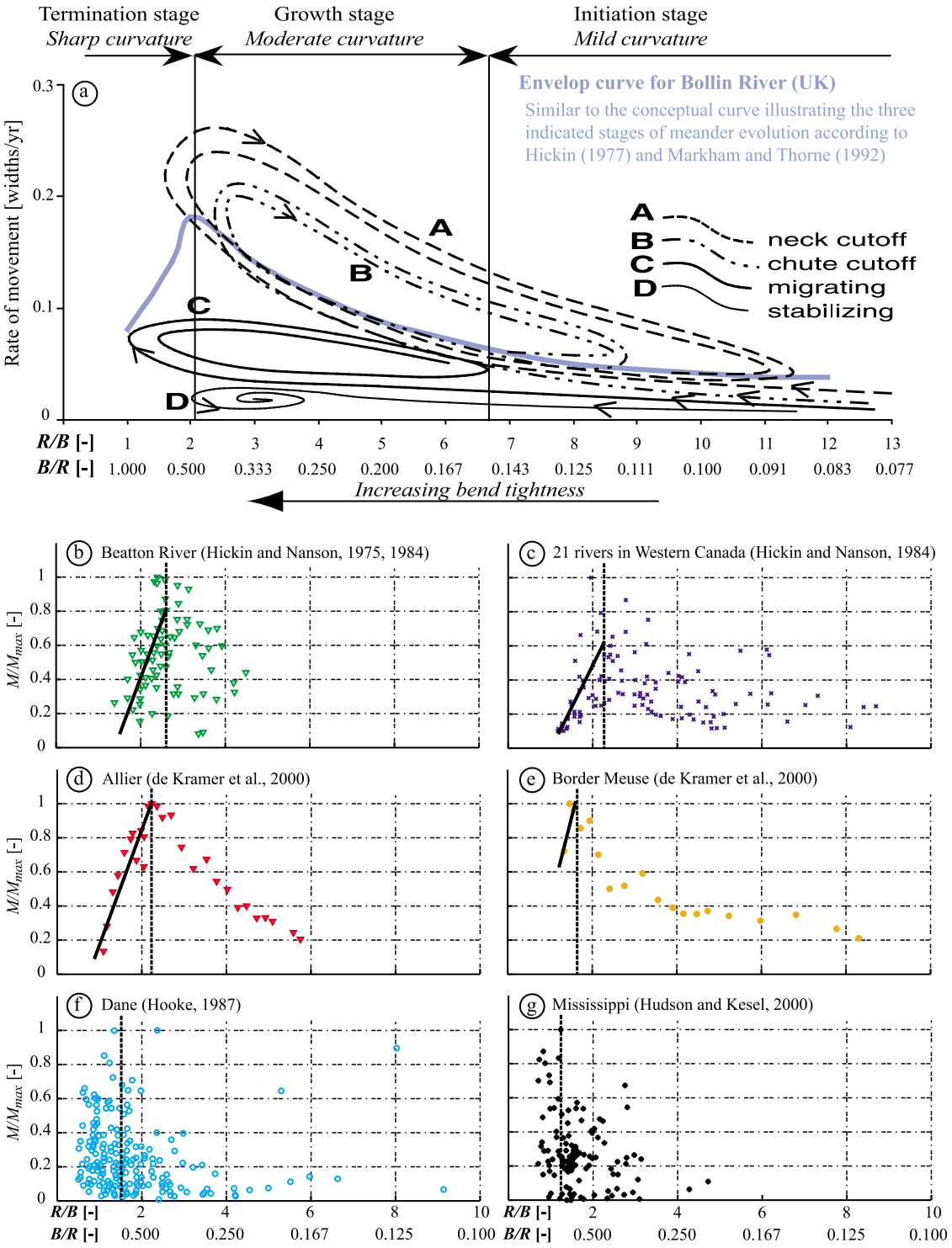

Figure 2. (a) Conceptual model for the three stages of meander evolution according to *Hickin* [1977] and *Markham and Thorne* [1992] and conceptual model for the different types of meandering according to *Hooke* [2003]. (b–g) Field data (see legend) on the normalized outer-bank migration rate M/M_{max} as function of meander curvature, parameterized by ratio of width to centerline radius of curvature, B/R.

et al., 2009] invariably describe the magnitude of the secondary flow as being proportional to the ratio H/R; therefore they are called linear models. Nonlinear hydrodynamic interactions are known to limit the growth of the secondary flow with increasing curvature [*de Vriend*, 1981; *Yeh and Kennedy*, 1993]. *Blanckaert* [2009] shows that the secondary flow does not increase when the curvature is increased in very sharp bends, and he called this process the saturation of the secondary flow. This process has been observed in sharp bends of natural peatland channels by *Nanson* [2010].

Table 1. Suggested Causes of the Apparent Maximum Meander Migration Rate (Figure 2)

Suggested Causes	Reference
Flow separation at the (convex) inner bank	*Bagnold* [1960]
Flow separation at the (concave) outer bank and the formation of outer-bank benches	*Hickin* [1977, 1978], *Hickin and Nanson* [1984], *Markham and Thorne* [1992]
Minimum energy expenditure	*Chang* [1984]
Maximum radial force per unit area exerted by the flow on the outer bank	*Begin* [1981, 1986]
Local obstructions in the floodplain, interactions between nonperiodic adjacent bends and higher-order flow interactions	*Parker and Andrews* [1986]
Interplay between the migrating river and the changing sedimentary environment created by the meandering river itself	*Sun et al.* [1996]
Nonlinear interactions between the flow, the bed topography and the river planform	*Seminara et al.* [2001]
Spatial lag between the local curvature and the location of the maximum velocity excess	*Seminara* [2006], *Crosato* [2008]
Saturation of the curvature-induced secondary flow	present paper
Outer-bank cells of secondary flow	present paper

Section 3 investigates how the saturation of the secondary flow affects the velocity excess and the meander migration rate.

[12] 2. Additional secondary flow cells, called outer-bank cells (Figure 1), are known to occur in the region near the outer bank and to play an important role with respect to the stability of the outer bank and the adjacent bed [*Bathurst et al.*, 1979; *Blanckaert and Graf*, 2004]. Section 4 will review current knowledge on outer-bank cells and investigate their conditions of occurrence, the dependence on the curvature, their evolution around a bend and their relevance to meander migration.

[13] 3. Section 5 will report detailed measurements on (horizontal) flow separation at the inner bank that provide insight into the characteristics of flow separation, the interaction with a mobile bed and the implications for meander migration.

[14] The investigation of these three processes combines laboratory experiments (section 2) with theoretical analysis using *Blanckaert and de Vriend*'s [2003, 2010] reduced-order nonlinear hydrodynamic model for flow in sharp meander bends (section 3).

2. Laboratory Experiments

[15] Obviously, the large variety of meander configurations encountered in nature renders the definition of a representative laboratory configuration impossible. Field investigations typically parameterize curvature effects by the unique curvature ratio B/R (Figure 2), which was identified by *Hickin* [1974] and *Hickin and Nanson* [1975] as the dominant control parameter for morphological processes. According to *Blanckaert and de Vriend*'s [2010] nonlinear model, however, $C_f^{-1}H/B$ and B/R are the dominant control parameters (see further in section 3). The former is a characteristic of a river that accounts for the shallowness and the roughness, whereas the latter parameterizes the curvature of individual bends. Table 2 estimates the value of the parameters $C_f^{-1}H/B$ and B/R in laboratory flumes and natural meandering rivers. The parameter $C_f^{-1}H/B$ is between 6 and 10 in most meandering rivers, and tends to decrease with increasing size of the river. Laboratory flumes with mobile bed are typically narrower and rougher than natural rivers, leading to similar values of $C_f^{-1}H/B$. Laboratory flumes with horizontal bed, on the contrary, are typically considerably smoother yielding higher values of $C_f^{-1}H/B$. This indicates that care should be taken with the extrapolation of results obtained in such configurations toward natural river configurations.

[16] Physical and numerical experiments are commonly performed in simplified schematized configurations that are designed based on the dominant control parameters. Such experiments isolate and/or accentuate certain parameters and processes under controlled conditions. The physical experiments reported in this paper were performed in a 1.3 m wide laboratory flume consisting of a 193° bend with a constant centerline radius of curvature of R = 1.7 m, preceded and followed by straight reaches 9 m and 5 m long, respectively. The bed was covered by a quasi-uniform sand with a diameter d = 0.002 m. Although the curvature ratio B/R = 0.79 is representative for sharp natural meander bends (Figure 2 and Table 2), some important differences exist with sharp natural meander bends that should be considered in the data interpretation and analysis. First, the centerline radius of curvature in the laboratory flume is constant in the bend and discontinuous at the bend entry and exit. This is not representative for natural meanders [*Güneralp and Rhoads*, 2009], although abrupt breaks, peaks and changes tend to be common features in natural meanders (as, for example, on the Embarras River investigated by *Frothingham and Rhoads* [2003]). Moreover, flow, and especially the morphology, adapt gradually to changes in curvature, which attenuates the effect of discontinuities in curvature. Therefore, the first half of the laboratory bend is representative of zones of pronounced curvature increase in meander bends, the second half of the bend is representative of zones of weak curvature variation, and the bend exit and straight outflow reach are representative of zones of pronounced curvature decrease. Second, the uniform flow over the width at the entry of the laboratory bend is not representative of natural meanders. The flow at the entry of natural bends is mainly determined by the upstream meander planform. Periodic meanders with alternating bends typically lead to a velocity decrease from the inner toward the outer bank at the bend entry. But the infinity of meander planforms may give rise to other velocity distributions at the entry. Third, outer banks are typically steep in sharp meander bends [*Leopold and Wolman*, 1960; *Thorne et al.*, 1995] but not vertical and hydraulically smooth like in most of the investigated experiments (Table 3). Fourth, real meander bends are characterized by a pronounced cross-stream grain-size gradient, which differs from the quasi-uniform sediment over the width in the laboratory flume. The major contribution to flow resistance in meander bends does not stem from

Table 2. Estimates of the Parameters $C_f^{-1}H/B$ and B/R in Some Laboratory Flumes and Natural Meandering Rivers[a]

River or Laboratory Flume	Q (m^3 s^{-1})	B (m)	$C_f^{-1}H/B$	$(B/R)_{max}$	Source
Laboratory Flumes					
Kinoshita laboratory flume at UIUC, horizontal bed	0.050 0.025	0.6 0.6	68.5 46.7	0.89 0.89	*Abad and Garcia* [2009a]
Large single bend laboratory flume at EPFL, horizontal bed					
F_21_90_00 experiment	0.104	1.3	37.7	0.76	present paper
F_16_90_00 experiment	0.089	1.3	26.4	0.76	present paper
F_16_30_30 experiment	0.078	1.16	22.8	0.68	present paper
F_16_90_30 experiment	0.089	1.3	21.2	0.76	present paper
F_11_90_00 experiment	0.056	1.3	18.0	0.76	present paper
Small single bend laboratory flume at EPFL, mobile bed	0.017	0.4	34.7	0.20	*Blanckaert and Graf* [2001, 2004]
Single bend flume at Delft University of Technology, horizontal bed	0.0052	0.5	27.4	0.12	*Booij* [2003]
Single bend flume at Univ. Ottawa., mobile bed	0.072	1	23.6	0.67	*Post and Rennie* [2007]
Sine-generated flume at Queens Univ., mobile bed	0.011–0.006	0.8	25.2–9.3	1.01	*Ferreira da Silva and El-Tahawy* [2008]
Kinoshita laboratory flume at UIUC, mobile bed	0.025	0.6	12.2	0.89	*Abad and Garcia* [2009b]
Single bend flume, UPC, mobile bed	0.041	1.0	12.0	0.67	*Roca et al.* [2009]
Large single bend laboratory flume at EPFL, mobile bed, M_16_90_00 experiment	0.089	1.3	8.6	0.76	present paper
Single bend flume at Univ. Iowa, mobile bed	0.153	2.27	7.9	0.17	*Odgaard and Bergs* [1988]
Sine-generated flume at Queens Univ., horizontal bed	0.00201 0.00184	0.4 0.4	8.0 5.7	0.52 0.81	*Ferreira da Silva et al.* [2006]
Sine-generated flume at Univ. California., mobile bed	0.000940 0.000422	0.25 0.125	4.3 3.7	0.35 0.51	*Whiting and Dietrich* [1993]
Natural Rivers					
Polblue Creek bend 3 (Australia)	0.3	1.3	54.9	1.2	*Nanson* [2010]
Savannah (USA)	860	107	20.7		*Crosato* [2008]
Dommel (The Netherlands)	1.5	6	12.2	0.59	*de Vriend and Geldof* [1983]
Geul at Mechelen (The Netherlands), bankfull	22	8	10.2		*Crosato* [2008]
Three Mile Slough (USA)	1400	200	9.4	1	*Fong et al.* [2009]
Fall River (Colorado, USA), bankfull	6.1	10.8	9.1	0.79	*Jackson* [1992]
Allier upstream of Moulins (France), bankfull	325	65	9.0		*Crosato* [2008]
Waal River (Lower Rhine branch, The Netherlands), 1998 flood	6500	335	7.9		*Julien et al.* [2002]
Dhaleswari River (Bangladesh), bankfull	1300	300	7.0		*Crosato* [2008]
Rhine River (The Netherlands), 1998 flood	9000	420	6.1		*Julien et al.* [2002]
East Nishnabotna River (USA), bankfull	120	50	6.0		*Odgaard* [1984]
Victoria Bendway on the Mississippi River at the confluence with the White River (USA), bankfull in main channel	12600	380	5.4	0.3	*Jia and Wang* [2000]
Muddy Creek (USA)	1.6	5.5	5.3	0.67	*Dietrich and Smith* [1983]

[a]In descending order of $C_f^{-1}H/B$.

the grain roughness, however, but from the form drag provided by mesoscale (bed forms) and macroscale (point bar/riffle and pool) topographic features.

[17] Hydrodynamic processes in sharp meander bends were investigated in the laboratory flume by means of measurements of flow and turbulence with high spatial and temporal resolution with an Acoustic Doppler Velocity Profiler [*Hurther*, 2001; *Blanckaert and Lemmin*, 2006; *Blanckaert*, 2010]. *Blanckaert* [2010] reports detailed information on the ADVP, the data processing and estimates of the uncertainty in the data. A series of 12 experiments [*Blanckaert*, 2002; *Duarte*, 2008] was performed that systematically investigated the influence of a single parameter, while the other parameters were held constant. Table 3 summarizes the main parameters of the 6 experiments illustrated in the present paper. Flow in all experiments was subcritical ($Fr < 1$) and rough turbulent ($Re^* = u^* k_s/\nu > 70$ where Nikuradse's equivalent sand roughness k_s has been defined according to *van Rijn* [1984] as three times the sand diameter). The hydraulic conditions in the M_16_90_00

Table 3. Hydraulic and Geometric Conditions in the Series of Experiments[a]

Label	Q (m^3 s^{-1})	q_s (kg s^{-1} m^{-1})	$\tilde{H}$ (m)	$\tilde{U}$ (m s^{-1})	$C_f^{-1/2}$	Re (10^3)	Fr	R/B	R/H	B/H	k_s, bank (m)	Θ_{bank} (deg)
F_11_90_00	56		0.108	0.40	14.7	43	0.39	1.31	15.6	12.1	PVC	90
F_16_90_00	89		0.159	0.43	14.7	69	0.35	1.31	10.6	8.2	PVC	90
F_21_90_00	104		0.206	0.38	15.2	81	0.26	1.31	8.0	6.1	PVC	90
M_16_90_00	89	0.023	0.141	0.49	14.0	68	0.41	1.31	12.1	9.2	PVC	90
F_16_90_30	89		0.155	0.44	13.2	69	0.35	1.31	10.6	8.2	0.030	90
F_16_30_30	78		0.156	0.43	12.8	69	0.35	1.46	10.6	7.2	0.030	30

[a]Q is the flow discharge, q_s is the sediment discharge, $\tilde{H}$ is the flume-averaged flow depth, $\tilde{U} = Q/B\tilde{H}$ is the flume-averaged velocity, $C_f^{-1/2} = U/\sqrt{gR_hE_s}$ is a Chézy-type friction coefficient for the straight inflow based on the hydraulic radius R_h and the measured streamwise energy gradient E_s, $Re = \tilde{U}\tilde{H}/\nu$ is the Reynolds number, $Fr = \tilde{U}/\sqrt{g\tilde{H}}$ is the Froude number, B is the flume width, $k_{s,bank}$ is the roughness diameter of the outer bank material, and Θ_{bank} is the inclination of the outer bank. Notations in the text are simplified by dropping the tildes on flume-averaged values.

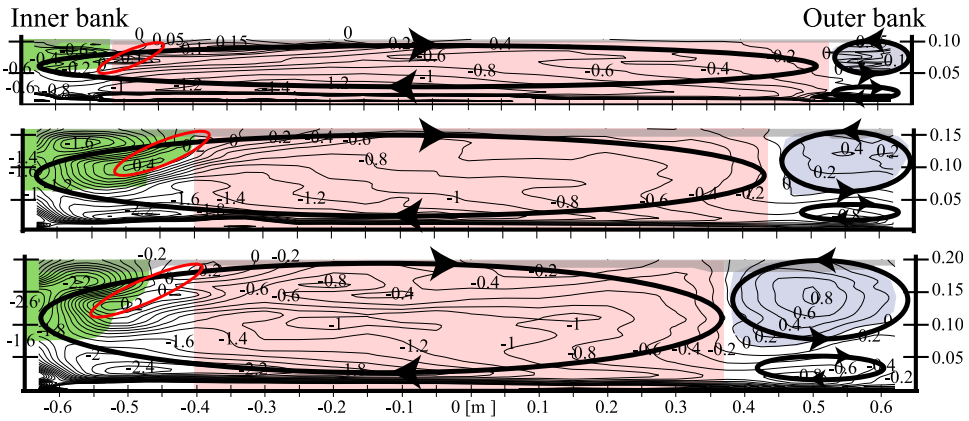

name	section	H/R	center-region cell (average in vertical with maximum values)		outer-bank cell	
			$(\omega_s H/U)$	$\frac{(\omega_s H/U)}{H/R}$	$(\omega_s H/U)$ mean / maximum	$\frac{(\omega_s H/U)}{H/R}$ mean / maximum
F_11_90_00	135°	0.064	-0.36	-5.64	0.07 / 0.15	1.09 / 2.34
F_16_90_00	90°	0.094	-0.45	-4.83	0.17 / 0.43	1.81 / 4.57
F_21_90_00	75°	0.125	-0.39	-3.15	0.35 / 0.83	2.80 / 6.64

Figure 3. Measured patterns of the secondary flow quantified by the normalized streamwise component of the vorticity, $\omega_s H/U$ in the F_11_90_00, F_16_90_00 and F_21_90_00 experiments. The patterns are shown in the cross section at 135°, 90°, and 75° in the bend in the respective experiment, where the secondary flow reaches its maximum magnitude according to centerline measurements reported by *Blanckaert* [2009]. A schematic pattern of the center-region and outer-bank cells of secondary flow, whose separation is inferred from the contour of zero streamwise vorticity, is shown. The green area corresponds to the zone of inner-bank flow separation; its delimiting shear layer is inferred from the inflexion point in the streamwise velocity distribution. The red contour indicates a zone of opposite vorticity inside the center-region cell of secondary flow located on the shear layer due to the inner-bank flow separation. The table quantifies the strength of the secondary flow cells as a function of the ratio H/R. The experimental uncertainty is estimated as less than 20%. The images are drawn at undistorted scales.

experiment with mobile bed were chosen such that the control parameters B/R = 0.76 and $C_f^{-1}H/B$ = 8.6 agreed well with typical values in sharp natural meander bends (Table 2), and such that representative mesoscale (bed forms) and macroscale (point bar and pool) topographic features developed. Similar hydraulic conditions were adopted in the F_16_90_00 experiment over a horizontal bed to investigate the influence of the bed morphology, and in the F_16_30_30 and F_16_90_30 experiments to explore the influence of the roughness and the inclination of the outer bank. Different discharges and flow depths in the F_11_90_00, F_16_90_00, F_21_90_00 provided information on the effect of the ratio H/R, which was identified as the dominant scaling parameter for secondary flow. The influences of the outer bank configuration and the ratio H/R were investigated over a fixed horizontal bed to avoid confounding effects of the bed morphology. Similar to horizontal bed experiments reported in literature, the parameter $C_f^{-1}H/B$ = 18.0 to 37.7 was outside of the range typical for natural sharp meander bends (Table 2). These horizontal bed experiments, however, do not intend to mimic the global hydrodynamic and morphologic behavior of natural meander bends. Their objective is to reproduce and investigate isolated hydrodynamic processes (saturation of the secondary flow and outer-bank cells of secondary flow) that occur in sharp bends. Sections 3, 4, and 5 discuss the effect of these differences between the laboratory flume and natural sharp meander bends on the data interpretation and morphological implications.

3. Saturation of Curvature-Induced Secondary Flow

[18] As discussed in the introduction, reduced-order mathematical models for meander migration are largely driven by the secondary flow, which they prescribe as being proportional to the ratio H/R; therefore these models are called linear models. These models overpredict secondary flow [*Blanckaert and de Vriend*, 2003; *Blanckaert*, 2009], and their validity range is limited because they are based on the hypotheses that (1) the curvature is mild, (2) the curvature only varies slowly through the bend, and (3) nonlinear hydrodynamic interactions are negligible.

[19] Nonlinear hydrodynamic interactions limit the growth of the secondary flow with increasing curvature [*de Vriend*, 1981; *Yeh and Kennedy*, 1993]. *Blanckaert* [2009] shows that the secondary flow does not increase with curvature in very sharp bends, and he called this process the saturation of the secondary flow. This process is illustrated in Figure 3,

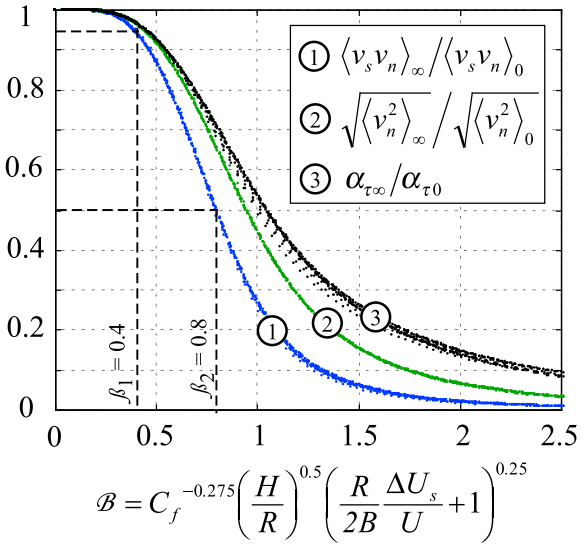

Figure 4. Solution of *Blanckaert and de Vriend*'s [2003, 2010] nonlinear model in the form of a correction coefficient to be applied to the linear model solutions. The index "∞" indicates fully developed conditions, whereas the index "0" indicates linear model solutions. Modified from *Blanckaert and de Vriend* [2003].

which shows patterns of the secondary flow quantified by means of the streamwise vorticity component, $\omega_s = \partial v_z/\partial n - \partial v_n/\partial z$, in the F_11_90_00, F_16_90_00 and F_21_90_00 experiments. The curvature-induced secondary flow in the central part of the cross section, called center-region cell, clearly shows saturation, as indicated by its comparable magnitude in the three experiments (differences are within the estimated experimental uncertainty of about 20%; see also the recapitulating table inserted in Figure 3), in spite of the considerable increase in the ratio H/R.

[20] *Blanckaert and de Vriend* [2003, 2010] have proposed and validated a reduced-order nonlinear hydrodynamic model that accounts for nonlinear hydrodynamic interactions and that has no restrictions in the magnitude of the curvature and its variations through the bend. This model satisfactorily resolves the center-region cell of secondary flow, its saturation at strong curvature, the velocity redistribution along the bend and the velocity excess $\Delta U_s/U$ at the outer bank [*Blanckaert and de Vriend*, 2003, 2010]. The nonlinear model solutions are obtained by computing the linear model solutions (index 0) and subsequently applying nonlinear correction factors according to the curves shown in Figure 4. These curves show that the nonlinear correction factors uniquely depend on the so-called bend parameter $\mathcal{B}$:

$$\mathcal{B} = C_f^{-0.275}\left(\frac{H}{R}\right)^{0.5}\left(\frac{R}{2B}\frac{\Delta U_s}{U}+1\right)^{0.25} \tag{2}$$

The dependence on the velocity excess $\Delta U_s/U$ is particularly important in the context of the reported analysis. According to Figure 4, nonlinear hydrodynamic effects are negligible ($\mathcal{B}$ = 0) when $\Delta U_s/U = -2B/R$. This corresponds to a potential-vortex velocity distribution characterized by maximum velocities at the inner bank, and is a reasonable lower bound for the velocity excess $\Delta U_s/U$. According to equation (2) and Figure 4, nonlinear hydrodynamic effects remain small when the velocity decreases from the inner toward the outer bank, $\Delta U_s/U < 0$, and only become important when velocities increase from the inner toward the outer bank, $\Delta U_s/U > 0$. Reference is made to *Blanckaert and de Vriend* [2003, 2010] for a detailed presentation, validation and discussion of their model as well as a comparison to the most recent and complete reduced-order hydrodynamic models [*Odgaard*, 1989; *Johannesson and Parker*, 1989a; *Imran et al.*, 1999; *Zolezzi and Seminara*, 2001; *Bolla Pittaluga et al.*, 2009].

[21] *Blanckaert and de Vriend*'s [2003, 2010] model provides a theoretical tool for assessing the influence and relevance of nonlinear hydrodynamic effects on the magnitude of the secondary flow, the velocity excess and the meander migration rate. To obtain generic results whose validity is not limited to one particular meander planform, two idealized configurations will be analyzed, and the relevance of the results to natural meander bends will subsequently be discussed.

[22] 1. The parameter space will first be reduced by considering fully developed (also called axisymmetric, or infinite bend) conditions where by definition no streamwise gradients occur in geometric and hydraulic characteristics. Nonlinear hydrodynamics effects are greatest in this configuration because the flow has completely adapted to the curvature and is characterized by velocities that increase from the inner toward the outer bank (equation (2) and Figure 4).

[23] 2. Sine-generated meanders will subsequently be considered, which are a kind of averaged idealized representation of the planform of natural meandering rivers [*Leopold and Wolman*, 1960]. In sine-generated meanders the change in direction of curvature from one bend to the next causes the velocity distribution at the bend entrance to be maximum at the inner bank. The core of maximum velocity gradually moves outward toward the outer bank at the exit of the bend. This velocity pattern, which is typical of that found in natural meander bends, minimizes nonlinear hydrodynamic effects (equation (2) and Figure 4).

3.1. Fully Developed Conditions

[24] According to equation (1) the meander migration rate is proportional to the velocity excess at the outer bank $\Delta U_s/U$, which *Blanckaert and de Vriend*'s [2010] model determines in fully developed conditions (indicated by the index "∞") by the following set of equations:

$$\frac{\Delta U_{s,\infty}}{U} = \left(Fr_\infty^2 + A_\infty - 1\right)\frac{B}{4R} + \frac{3}{\psi_\infty}\frac{1}{C_f}\frac{H}{B}\frac{\langle v_s v_n\rangle_\infty}{U^2} \cdot \left[1 + \frac{1}{12}\frac{B^2}{R^2}\left(Fr_\infty^2 + A_\infty + 3\right)\right] \tag{3}$$

$$Fr^2 + A = \frac{(1+n/R)R}{h}\frac{\partial h}{\partial n} \overset{\text{linear approximation}}{\approx} \frac{R}{H}\frac{\partial h}{\partial n} \tag{4}$$

$$A_\infty = \alpha_{\tau,\infty}/G \tag{5}$$

$$\alpha_{\tau,\infty} = \frac{\tau_{bn}}{\tau_{bs}}\Big/\frac{H}{R} \tag{6}$$

$$\begin{cases} A_\infty \overset{\text{Equation (5)}}{=} \dfrac{\alpha_{\tau,\infty}}{\alpha_{\tau,0}} \quad A_0 \overset{\substack{\text{Figure (4)}\\ \text{Equation (5)}}}{=} \mathrm{fct}_3(\mathcal{B}) \quad \dfrac{\alpha_{\tau,0}}{G} \\ \dfrac{\langle v_s v_n\rangle_\infty}{U^2} = \dfrac{\langle v_s v_n\rangle_\infty}{\langle v_s v_n\rangle_0} \dfrac{\langle v_s v_n\rangle_0}{U^2} \overset{\text{Figure (4)}}{=} \mathrm{fct}_1(\mathcal{B}) \dfrac{\langle v_s v_n\rangle_0}{U^2} \\ \dfrac{\sqrt{\langle v_n^2\rangle}_\infty}{U} = \dfrac{\sqrt{\langle v_n^2\rangle}_\infty}{\sqrt{\langle v_n^2\rangle}_0} \dfrac{\sqrt{\langle v_n^2\rangle}_0}{U} \overset{\text{Figure (4)}}{=} \mathrm{fct}_2(\mathcal{B}) \dfrac{\sqrt{\langle v_n^2\rangle}_0}{U} \end{cases} \quad (7)$$

The index "0" indicates linear-model solutions. The parameter ψ, provided by *Blanckaert and de Vriend*'s [2003, 2010] model, parameterizes additional curvature-induced friction losses. The brackets $\langle\ \rangle$ indicate depth-averaged values. According to equation (4), the square of the Froude number, Fr^2, and the so-called scour factor A [*Engelund*, 1974; *Zimmerman and Kennedy*, 1978; *Odgaard*, 1981] parameterize the transverse slopes of the water surface and the bed, respectively. *Olesen* [1987] summarizes models for the coefficient G (equation (5)), which quantifies the gravitational downslope pull on sediment particles situated on a transverse inclined bed. The coefficient α_τ (equations (5) and (6)) quantifies the transverse component of the bed shear stress τ_{bn} induced by the secondary flow (Figure 1). The quantity $\sqrt{\langle v_n^2\rangle}/U$ (equation (7)) is a dimensionless measure of the magnitude of the secondary flow.

[25] Equations (3) to (7) clearly reveal the processes underlying the velocity excess at the outer bank and the important role played by the secondary flow. Equation (5) expresses that the transverse bed slope A in fully developed conditions is the result of equilibrium between the gravitational downslope pull on the sediment particles and the upslope drag force induced by the secondary flow, represented by G and α_τ, respectively. When adopting linear approximations of the transverse water surface and bed slopes (equation (4)), the flow depth excess at the outer bank is given by $\Delta h/H = [Fr^2 + A]B/(2R)$, where H is the average flow depth in the cross section. This flow depth excess at the outer bank determines the first term in equation (3) for the velocity excess. It indicates that higher/lower flow depths lead to higher/lower velocities, a phenomenon that is often called topographic steering. *Blanckaert and de Vriend* [2010] have shown that this first term is an extension of Chézy's formula for straight uniform flow, which expresses $U \sim \sqrt{h}$. The second term in equation (3) is proportional to $\langle v_s v_n\rangle$, which represents the redistribution of streamwise velocity v_s by the secondary flow v_n. Outward redistribution in the upper half of the water column is typically larger than inward redistribution in the lower part of the water column (Figure 1). Averaged over the flow depth, this results in net outward transfer of momentum.

[26] The saturation of the secondary flow due to nonlinear hydrodynamic effects directly affects both processes underlying the velocity excess at the outer bank. It leads to reductions in the transverse bed slope (A, first term in equation (3)) and in the momentum redistribution by the secondary flow ($\langle v_s v_n\rangle$, second term in equation (3)) that *Blanckaert and de Vriend*'s [2003, 2010] model quantifies by means of nonlinear correction coefficients (defined in equation (7) and illustrated in Figure 4). Inclusion of these correction coefficients makes the variables $\Delta U_s/U$, A and $\langle v_s v_n\rangle$ mutually dependent according to equations (2), (3) and (7), indicating the nonlinearity of the hydrodynamics.

[27] A mild-curvature formulation of *Blanckaert and de Vriend*'s [2003, 2010] model is obtained by neglecting the last term between square brackets in equation (3) and by setting fct(β) = 1 (equation (7)), which renders A and $\langle v_s v_n\rangle$ independent of $\Delta U_s/U$ and proportional to the ratio H/R. This mild-curvature formulation is identical to the linear model of *Johannesson and Parker* [1989a]. Comparison of Blanckaert and de Vriend's model without curvature restrictions to the model of *Johannesson and Parker* [1989a] therefore reveals the influence and relevance of nonlinear hydrodynamic effects. Extensions and improvements of Johannesson and Parker's model have been proposed by, e.g., *Imran et al.* [1999], *Zolezzi and Seminara* [2001], and *Bolla Pittaluga et al.* [2009]. Comparison to these models would lead to similar results, however, because they are all based on the assumptions of mild curvature and slow curvature variations [*Blanckaert and de Vriend*, 2010].

[28] As already discussed in section 2, equation (3) identifies $C_f^{-1}H/B$ and B/R as the two dominant control parameters with respect to the velocity excess at the outer bank in fully developed conditions. The former is a characteristic of a river, whereas the latter parameterizes the curvature of individual bends. Figures 5 and 6 show the magnitude of the secondary flow and the velocity excess, respectively, as a function of $C_f^{-1}H/B$ and B/R according to *Blanckaert and de Vriend*'s [2003, 2010] model without curvature restrictions (Figures 5 (left) and 6 (left)) and according to the model in its linear mild-curvature formulation (Figures 5 (right) and 6 (right)). The simulations account for the effect of the transverse bed slope by means of a scour factor of $A_0 = 4$, which is within the range of 2.5 to 6 that is typical for natural rivers according to *Odgaard* [1981] and *Ikeda et al.* [1981]. Moreover a typical friction factor for natural rivers of $C_f = 0.0157$ has been adopted. It should be noted, however, that the choice of the scour and friction factors does not substantively affect the results.

[29] The mild-curvature model predicts the secondary flow to be proportional to the ratio H/R, which results in a monotonic increase as a function of B/R and $C_f^{-1}H/B$ (Figure 5, right). The model without curvature restrictions simulates the saturation of the secondary flow at high curvature as functions of B/R and $C_f^{-1}H/B$. It predicts an increase in the maximum magnitude of the secondary flow with B/R and $C_f^{-1}H/B$ in the parameter range typical for rough shallow natural rivers. In the parameter range typical for small, relatively deep natural rivers and laboratory flumes, the nonlinear effects are so strong that the magnitude of the secondary flow decreases in bends with increasing B/R and $C_f^{-1}H/B$. Differences between the model without curvature restrictions and the mild-curvature model can reach 100% in sharply curved large natural rivers, and even an order of magnitude in sharply curved laboratory flumes where the mild-curvature model predicts secondary flow velocities that are higher than the streamwise velocity, which is physically not possible and clearly indicates the limited validity of the mild-curvature models. Even in the sharpest bends, the secondary flow never exceeds $\sqrt{\langle v_n^2\rangle}/U > 0.15$ in fully developed conditions according to the model without curvature restrictions. It should be noted that the secondary flow typically "overshoots" its

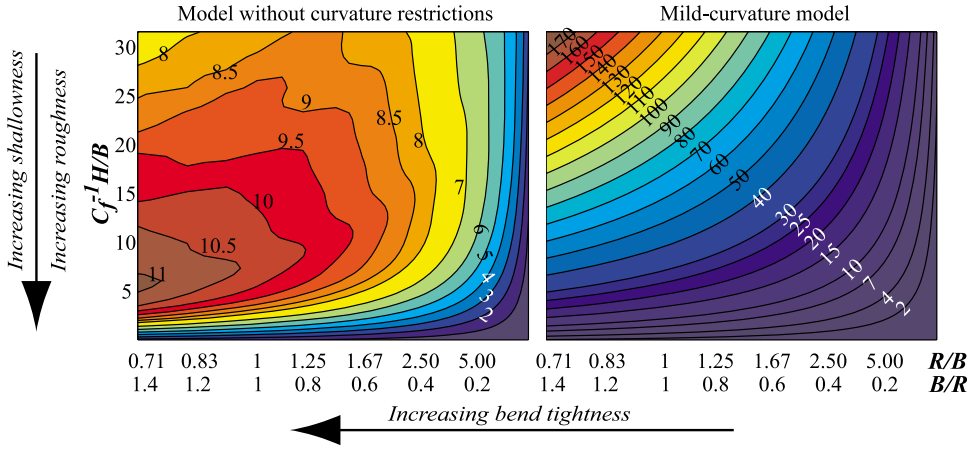

Figure 5. Normalized magnitude of the center-region cell of secondary flow $100\sqrt{\langle v_n^2 \rangle}/U$ in fully developed conditions as a function of the parameters B/R and $C_f^{-1}H/B$ according to *Blanckaert and de Vriend*'s [2003, 2010] model: (left) without curvature restrictions and (right) in its mild-curvature formulation. Note that the color scales in Figures 5 (left) and 5 (right) are different.

fully developed value in developing curved flow and reaches maximum values that are considerably higher (see *Blanckaert and de Vriend* [2003] and *Blanckaert* [2010] for configurations with horizontal and mobile bed topography, respectively).

[30] The mild-curvature model also predicts the velocity excess to increase monotonically as a function of B/R and $C_f^{-1}H/B$ (Figure 6, right). For a river with a specific value of $C_f^{-1}H/B$, the model without curvature restrictions predicts a saturation of the velocity excess when bends get sharper as parameterized by increasing values of B/R. With the exception of shallow and rough meandering rivers characterized by $C_f^{-1}H/B < 5$, the velocity excess even decreases in very sharp bends, which is in agreement with the meander migration rate observed in stabilizing meanders (Figure 2). The model predicts the curvature ratio where the maximum velocity excess and bank migration rate occur, $B/R_{M\max}$, to decrease with increasing $C_f^{-1}H/B$ (curve in Figure 6 (left)). For the range typical of natural meander bends ($C_f^{-1}H/B$ = 6 to 10) (Table 2), the predicted value $B/R_{M\max}$ = 0.5 to 1 agrees well with field observations reported in Figure 2. Contrary to the mild-curvature model, the model without curvature restrictions predicts the velocity excess to decrease monotonically with $C_f^{-1}H/B$ in sharp bends with $B/R > 0.5$. Differences between the model without curvature restrictions and the mild-curvature model increase monotonically with both B/R and $C_f^{-1}H/B$ and can reach 100% in sharply curved large natural rivers, and even an order of magnitude in sharply curved small natural rivers and laboratory flumes. The validity of mild-curvature models is limited to mildly curved bends, $B/R < 0.2$ in very rough and shallow natural rivers with $C_f^{-1}H/B < 2$. The validity of both models is limited to a maximum value of the velocity excess of 1, which would lead to negative velocities at the inner bank that could be

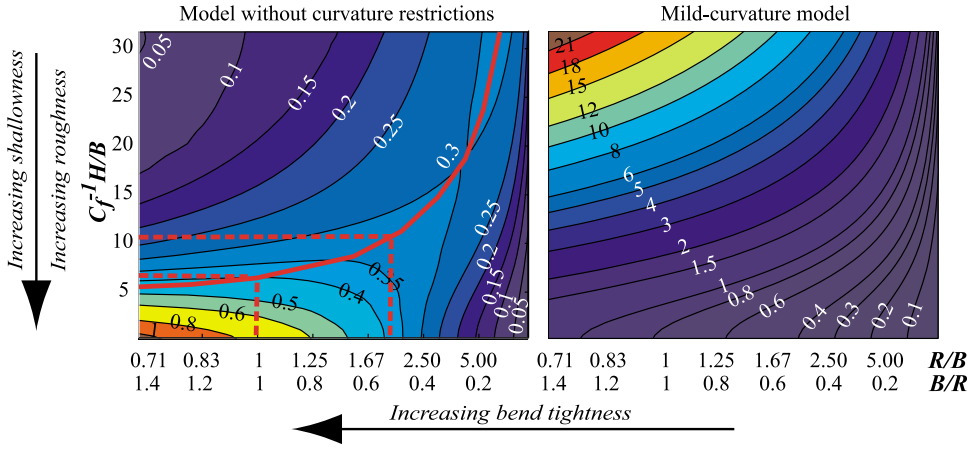

Figure 6. Velocity excess $\Delta U_s/U$ in fully developed conditions as a function of the parameters B/R and $C_f^{-1}H/B$ according to *Blanckaert and de Vriend*'s [2003, 2010] model: (left) without curvature restrictions and (right) in its mild-curvature formulation. The red line in Figure 6 (left) indicates the curvature ratio B/R at which the maximum migration rate occurs. Note that the color scales in Figures 6 (left) and 6 (right) are different.

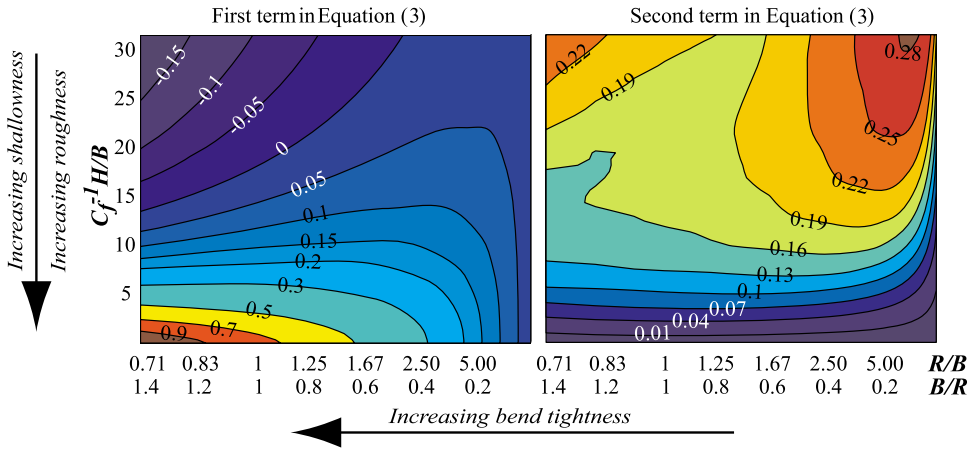

Figure 7. Dependence of the (left) first and (right) second terms in equation (3) for the velocity excess on the parameters B/R and $C_f^{-1}H/B$ according to *Blanckaert and de Vriend*'s [2003, 2010] model without curvature restrictions. Note that the color scales in Figures 7 (left) and 7 (right) are different.

interpreted as a first approximation of the onset of flow separation at the inner bank. The velocity excess predicted by the model without curvature restrictions never exceeds this limiting value, whereas the mild-curvature model yields physically impossible values that are an order of magnitude larger.

[31] To gain insight into the processes underlying the velocity excess, Figure 7 shows both terms in equation (3) as a function of B/R and $C_f^{-1}H/B$. The effect of the secondary flow on the velocity excess (Figure 7, right) scales with the parameter $C_f^{-1}H/B$ (equation (3)).Therefore it is small in shallow and rough bends in spite of the high magnitude of the secondary flow (Figure 5, left) and it is maximal in smooth and narrow bends of mild curvature, $B/R < 0.2$, despite the relatively low magnitude of the secondary flow (Figure 5, left). The effect of the transverse bed slope on the velocity excess (Figure 7, left), represented by the term $A_\infty B/R = (\alpha_{\tau,\infty}/\alpha_{\tau,0})A_0 B/R$ (equations (3) and (7)) is dominated by the saturation of the secondary flow, reflected in the ratio $(\alpha_{\tau,\infty}/\alpha_{\tau,0})$. The effect of the transverse bed slope only increases with B/R in rough and shallow bends with $C_f^{-1}H/B < 5$.

3.2. Sine-Generated Meanders

[32] According to *Leopold and Wolman* [1960] sine-generated meanders can be described by a sinusoidal variation of the centerline radius of curvature R:

$$\frac{1}{R(s)} = -\theta_0 \frac{2\pi}{L}\cos\left(2\pi\frac{s}{L}\right) \tag{8}$$

The value θ_0 is the maximum deflection angle with respect to the axis of the meander belt and L is the meander length along the centerline (Figure 8). *Ferguson* [1975] found an average ratio of L/B~20 for a sample of 19 rivers, which is consistent with the typical ratio of meander wavelength to width of Λ/B~2π given by *Leopold and Wolman* [1960]. The meander sinuosity, defined as the ratio between the meander length along the centerline and the meander wavelength is given by

$$\sigma = \frac{L}{\Lambda} = \frac{1}{J_0(\theta_0)} \tag{9}$$

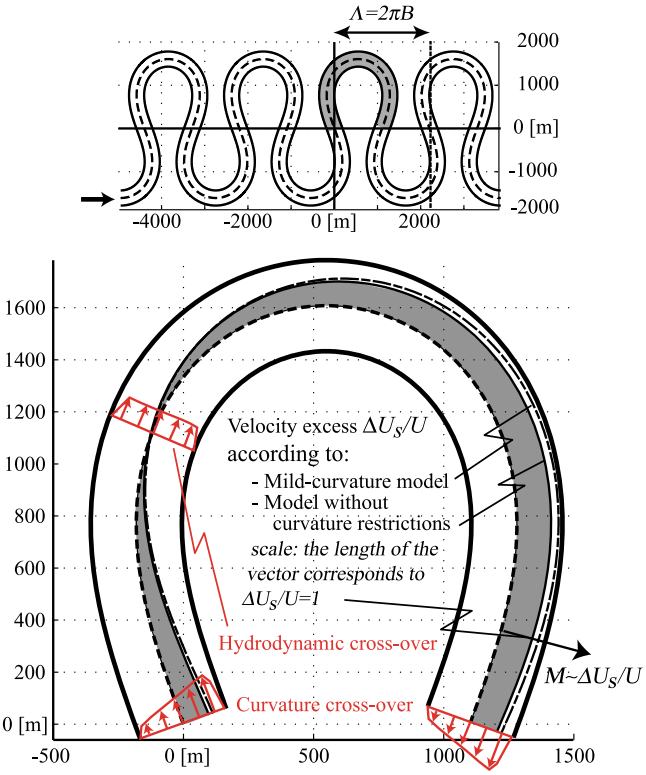

Figure 8. (top) Idealized sine-generated meander close to cutoff characterized by $\theta_0 = 110°$ and $B = 415$ m. (bottom) The normalized velocity excesses $\Delta U_s/U$ computed according to the model without curvature restrictions and the mild-curvature model are reported perpendicular to the centerline. Because the meander migration rate is proportional to the normalized velocity excess, $M\sim\Delta U_s/U$, this representation gives an indication of the new meander planform after meander migration. Figure 8 (bottom) also illustrates that the hydrodynamic crossover (transition between an upstream reach with locus of fastest flow at the inner side of the cross section and a downstream reach with locus of fastest flow at the outer side of the cross section) lags behind the curvature crossover (straight reach between two bends turning in opposite direction).

where $J_0(\theta_0)$ is the Bessel function of the first kind and zeroth order [*Ferguson*, 1973]. The maximum curvature ratio in the sine-generated meander is given by

$$\left(\frac{B}{R}\right)_{\max} = \theta_0 J_0(\theta_0) \tag{10}$$

A meander close to cutoff is characterized by high values of θ_0 of about 110°.

[33] The maximum velocity excess in idealized sine-generated meanders depends on the mean value of the curvature ratio B/R, the shallowness B/H and the friction coefficient C_f, which can no longer be regrouped into the two independent variables $C_f^{-1}H/B$ and B/R. The analysis using the model of *Blanckaert and de Vriend* [2003, 2010] employs geometric and hydraulic parameters representative of the Rhine River in the Netherlands, which is one of the largest European rivers and a major European waterway for navigation. During bankfull flow, it has a discharge of Q = 9000 m^3s^{-1}, a width of about 420 m, a flow depth of about 12 m and a dimensionless friction coefficient of about C_f = 0.0048 [*Julien et al.*, 2002], yielding dimensionless control parameters $C_f^{-1}H/B$ = 6.1, $(B/R)_{\text{mean}}$ = 0.33 and $(B/R)_{\max}$ = 0.52. Similar to the fully developed configuration, the bed topography is parameterized by A_0 = 4 in the mild-curvature model, which corresponds to a transverse bed slope that varies along the bend proportional to R^{-1} (equation (4)). *Johannesson and Parker* [1989b] have developed a theoretical justification for this simple but reasonable approximation. The model without curvature restrictions accounts for the effect of the saturation of the secondary flow on the transverse bed slope by means of $A = (\alpha_\tau/\alpha_{\tau 0})A_0$ (equation (7)).

[34] Figure 8 illustrates the initial sine-generated meander and compares the planforms after meander migration according to the model without curvature restrictions and the mild-curvature model. The meander migration, estimated as $M \sim \Delta U_s/U$, is reported perpendicular to the centerline. The maximum difference in migration rate between both models is about 15% and occurs in the region vulnerable to cutoff. This difference between the two models is only slightly smaller than the difference for fully developed conditions based on the average curvature ratio $(B/R)_{\text{mean}}$ = 0.33 (Figures 6 (left) and 6 (right)).

3.3. Natural Meander Bends

[35] *Blanckaert and de Vriend* [2010] performed a scaling analysis of the processes leading to the velocity excess at the outer bank in natural meander bends with varying curvature. They concluded that the influence of the transverse bed slope (first term in equation (3)) is always a process of leading order, irrespective of the bend geometry. Velocity redistribution by the secondary flow (second term in equation (3)) on the contrary, is a process of leading order in narrow rivers, $B/H < 10$, but negligible in very shallow ones, $B/H > 50$.

[36] Fully developed conditions are never encountered in natural meander bends where the flow and the bathymetry adapt to gradual changes in curvature. As a result, the secondary flow and the velocity excess lag behind the forcing by the centerline radius of curvature and never reach their fully developed values. *Güneralp and Rhoads* [2009], for example, formalize this inertial adaptation by means of a convolution function of the spatial distribution of curvature. Obviously nonlinear hydrodynamic effects will be more/less pronounced for shorter/longer spatial lags. The spatial lag strongly varies between bends since it depends on the planform (which defines the curvature variations, the width and the influences of upstream and downstream bends), the flow depth, the morphology and roughness. In the investigated sine-generated meander, the relatively low values of B/R and $C_f^{-1}H/B$ (Table 2), the slowly varying curvature and the inward skewed velocity distribution at the bend entrance provoke a long spatial lag, illustrated in Figure 8 by the distance between the curvature crossover and the hydrodynamic crossover. Nevertheless, the nonlinear hydrodynamic effects still considerably reduce the velocity excess. *Blanckaert and de Vriend* [2010] have validated their nonlinear model by means of the M_16_90_00 mobile-bed experiment and shown that the saturation of the secondary flow considerably reduces the velocity excess. As discussed in section 2, this experiment is quite representative for sharp natural meander bends, which are often short bends characterized by pronounced and abrupt changes in curvature. These cases indicate that nonlinear hydrodynamic effects and the resulting reduction in the velocity excess and the meander migration rate are always relevant in sharp natural meander bends, but strongly depend on the particular bend configuration. According to the analysis for fully developed conditions, the influence of nonlinear hydrodynamic effects can be expected to increase with B/R and $C_f^{-1}H/B$ indicating that large shallow rivers have the most dynamic meandering behavior, while the occurrence of stable meanders that do not evolve to the point of cutoff seems to be favored in small and relatively deep rivers.

4. Outer-Bank Cells of Secondary Flow

[37] Outer-bank cells (Figures 1 and 3) have been observed long ago in the laboratory [e.g., *Mockmore*, 1943; *Einstein and Harder*, 1954; *Rozovskii*, 1957] and in the field [e.g., *Hey and Thorne*, 1975; *Bridge and Jarvis*, 1977; *Bathurst et al.*, 1977, 1979; *Thorne and Hey*, 1979; *Dietrich and Smith*, 1983; *de Vriend and Geldof*, 1983; *Thorne et al.*, 1985; *Markham and Thorne*, 1992]. Recently, *Blanckaert and Graf* [2004] and *Blanckaert and de Vriend* [2004] have carried out detailed measurements of an outer-bank cell in a smaller laboratory flume with mobile-bed topography and vertical banks by means of the same Acoustic Doppler Velocity Profiles used in the experiments reported in this paper. The outer-bank cells are known to play an important role with respect to the stability of the outer bank and the adjacent bed. *Bathurst et al.* [1979] postulated that they endanger bank stability by advecting high-momentum fluid from near the water surface toward the lower part of the bank. *Blanckaert and Graf* [2004] found that they protect the outer bank and the adjacent bed by forming a buffer layer that protects the outer bank from any influence of the center-region cell. The center-region cell redistributes the velocity and causes it to increase toward the outer bank. The outer-bank cell prevents this increase to continue through to the bank and keeps the core of maximum velocity a distance from the bank at the separation between both cells.

[38] *Blanckaert and de Vriend* [2004] investigated the mechanisms underlying the generation of the outer-bank cell

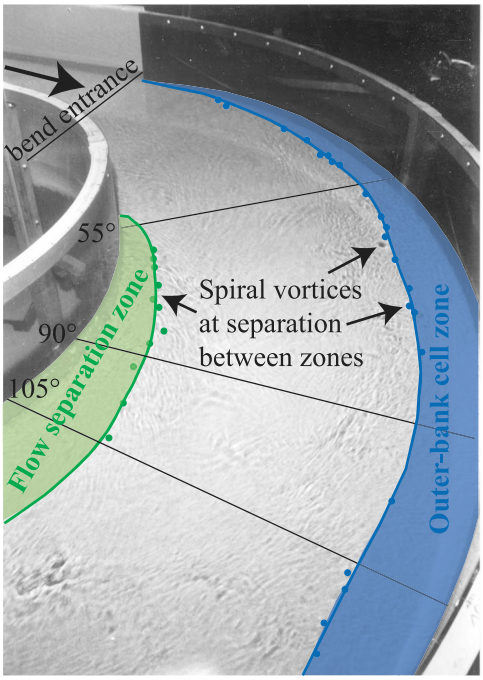

Figure 9. Visualization of the flow separation zone at the inner bank and the region covered by the outer-bank cell in the F_16_90_00 experiment (Figure 3).

by means of a term-by-term analysis of the balance equation for streamwise vorticity and the kinetic energy fluxes between the mean flow and the turbulence. Their results indicated that the outer-bank cell is generated by the mutually strengthening interaction of centrifugal effects and turbulence effects induced by the proximity of the water surface and the outer bank. The bed topography, on the contrary, was not found to play a dominant role. Therefore, experiments with a horizontal bed in the laboratory flume are appropriate for investigating outer-bank cells as well as their morphological implications, including:

[39] 1. Their dependence on the ratio H/R. From a long-term morphological point of view, H/R and the curvature ratio B/R are of constant proportion in natural meandering rivers, because the bankfull flow depth and the width are about constant for a river reach, whereas the centerline radius of curvature varies from one bend to another. Outer-bank cells are known to exist in mildly curved and sharply curved natural meander bends. However, little is known about their characteristics and possible differences in mildly and sharply curved meander bends.

[40] 2. Their evolution around a bend and their adaptation to changes in curvature.

[41] 3. Their conditions of occurrence and dependence on the roughness and inclination of the outer bank. *Bathurst et al.* [1977, 1979] and *Thorne and Hey* [1979], for example, postulate that outer-bank cells occur near steep banks but not near shelving ones.

[42] The first point is addressed in Figure 3, which shows the measured patterns of the secondary flow in the cross section where the center-region cell reaches its maximum magnitude in experiments with smooth vertical outer bank, but different values of the ratio H/R, which all correspond to very sharply curved flow. In all three experiments, the width of the outer-bank cells is comparable to the flow depth. Its strength, however, shows a pronounced, more than linear increase with the ratio H/R.

[43] The second point is addressed in Figure 9, which identifies the separation between the zones occupied by the center-region cell and the outer-bank cells by means of vertical spiral vortices in the F_16_90_00 experiments. Similar observations were made in the F_11_90_00 and F_21_90_00 experiments as well as in a natural meander bend by *Markham and Thorne* [1992]. The outer-bank cells' zone seems to come into existence at the bend entry and to widen in the first part of the bend, which is representative of zones of pronounced curvature increase in meander bends (section 2). Downstream of the cross section at about 60° in the bend, the outer-bank cell seems to retain a quasi-constant width. This zone is representative of meander bends with weak curvature variations (section 2). These observations are further confirmed by detailed measurements in 7 cross sections (15°, 30°, 60°, 90°, 120°, 150°, 180°) around the bend in the F16_90_00 experiment. Only measurements in the cross section at 90° in the bend will be reported in the present paper.

[44] The third point is addressed in Figure 10, which shows the measured patterns of the secondary flow in the cross section where the center-region cell reaches its maximum magnitude in an experiment with rough vertical bank and another with rough 30°-inclined bank, but with the same flow depth and a similar ratio H/R. The outer-bank cell widens and strengthens considerably with increasing roughness of the outer-bank, indicating that the outer-bank cell and its protective effect may be more important in natural meander bends with irregular rough banks than in laboratory or numerical experiments with smooth banks. Inclining the outer bank considerably weakens the outer-bank cell and changes its pattern. But its protective effect by forming a buffer layer between the outer bank and the center-region cell is conserved. According to *Leopold and Wolman* [1960] and *Thorne et al.* [1995], the outer bank in natural meander bends steepens when the curvature ratio B/R increases. As a result, the outer bank cell may be of minor importance with respect to bank erosion and meander migration in mildly curved meander bends and become relatively more important in very sharply curved meander bends.

5. Flow Separation and Recirculation at the (Convex) Inner Bank

[45] Flow separation at the (concave) outer bank and the associated formation of outer-bank benches are known to be important with respect to meander migration and the apparent maximum meander migration rate (Figure 2 and Table 1). *Hickin* [1977] reported that, on the Beatton River in western Canada, tight meander bends with very slow migration rate exhibit strong flow separation at the outer (concave) bank associated with the formation of concave-bank benches. Measurements on the Squamish River [*Hickin*, 1978] and on various rivers in western Canada [*Hickin and Nanson*, 1984] confirmed this observation. Also *Markham and Thorne* [1992] focused on flow separation at the outer bank and the formation of concave-bank benches to explain the apparent maximum migration rate.

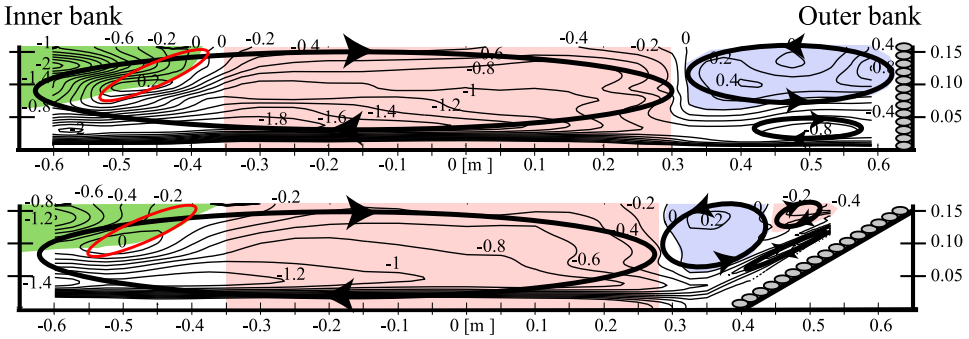

name	section	H/R	center-region cell (average in vertical with maximum values) $(\omega_s H/U)$	center-region cell (average in vertical with maximum values) $\frac{(\omega_s H/U)}{H/R}$	outer-bank cell $(\omega_s H/U)$ mean / maximum	outer-bank cell $\frac{(\omega_s H/U)}{H/R}$ mean / maximum
F_16_90_30	90°	0.094	-0.48	-5.31	0.21 / 0.73	2.23 / 7.73
F_16_30_30	90°	0.094	-0.49	-5.32	0.12 / 0.24	1.28 / 2.55

Figure 10. Measured patterns of the secondary flow quantified by the normalized streamwise component of the vorticity, $\omega_s H/U$, as a function of the outer bank roughness (compare to Figure 3) and inclination. Shown is a schematic pattern of the center-region and outer-bank cells of secondary flow, whose separation is inferred from the contour of zero streamwise vorticity. The green area corresponds to the zone of inner-bank flow separation; its delimiting shear layer is inferred from the inflexion point in the streamwise velocity distribution. The red contour indicates a zone of opposite vorticity inside the center-region cell of secondary flow located on the shear layer due to the inner-bank flow separation. The table quantifies the strength of the secondary flow cells as a function of the ratio H/R. The experimental uncertainty is estimated as less than 20%. The images are drawn at undistorted scales.

[46] Obviously, the constant width laboratory flume does not allow the investigation of flow separation at the outer bank related to the formation of outer-bank benches. Attention is henceforward restricted to flow separation and recirculation at the (convex) inner bank, which has been observed in natural meander bends by, e.g., *Bagnold* [1960], *Leeder and Bridges* [1975], *Ferguson et al.* [2003], and *Rhoads and Massey* [2010]. In spite of its importance with respect to meander migration, little is known about flow separation at the inner bank and its morphological implications. *Bagnold* [1960] suggested flow separation at the inner bank is at the origin of the apparent maximum meander migration rate in moderately curved bends. He argued that flow separation at the inner bank in bends of developing curvature concentrates the flow into the deeper outer part of the cross section where the relative roughness of the channel is less than over the shallow inaner bank zone. With further tightening of the bend, Bagnold argued that the inner-bank flow separation zone would become unstable and collapse, leading to an increase in flow resistance due to the flow that reoccupies the entire width of the cross section as well as a marked increase in macroturbulence. *Leeder and Bridges* [1975] also speculated that flow separation at the inner bank favors meander migration by reducing the effective width and directing high-velocity flow toward the outer bank. *Ferguson et al.* [2003], however, found that the reduced effective width is more than offset by an increase in flow depth and that the flow decelerates along the outer bank. *Leeder and Bridges* [1975] furthermore observed a rapid deposition of suspended sediment in the flow separation zone, which is expected to play an important role in the accretion at the inner bank. According to *Leeder and Bridges* [1975], flow separation is largely controlled by the curvature ratio B/R and the Froude number Fr, whereby an increase in bend tightness and Froude number favor flow separation. *Bagnold* [1960], on the contrary, rejected the use of the Froude number because separation in pipes is similar to separation in open-channel flows, but Fr can only be defined for open-channel flow. *van Balen et al.* [2010a] pointed to the critical role of turbulence in the generation of inner-bank flow separation.

[47] Besides the morphological implications and the parameters of influence, further knowledge gaps include the conditions of occurrence, the dependence on the streamwise variation in curvature, the dependence on the roughness and inclination of the inner bank, the mechanisms underlying flow separation, and the interaction of the hydrodynamics with a mobile bed. These knowledge gaps may largely be attributed to the lack of detailed measurements in the flow separation zone.

[48] The differences between the M_16_90_00 mobile bed experiment and natural sharp meander bends, discussed in section 2, are of minor importance with respect to inner-bank flow separation. Results are therefore representative for natural sharp meander bends. A sediment feeding rate of 0.023 kg m^{-1} s^{-1} led to the development of a dynamic state of equilibrium, characterized by steady macro features of the bathymetry with superimposed migrating dunes. In order to allow for detailed velocity measurements, the bathymetry

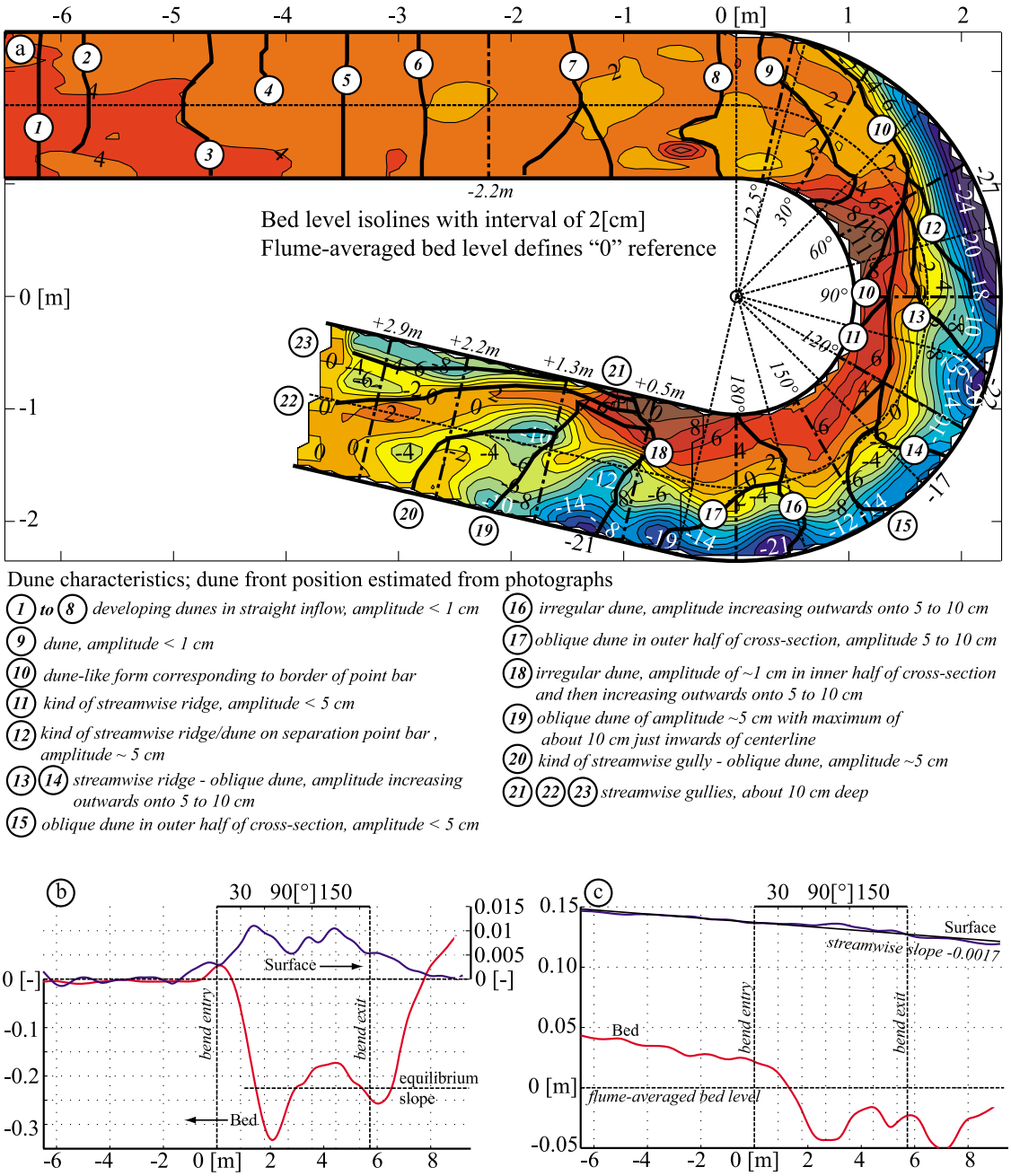

Figure 11. (a) Isolines of the bed level in the M_16_90_00 experiments with an interval of 0.02 m derived from echosounder measurements. Additional ADVP measurements with higher spatial resolution are available in the indicated cross sections. The position of dunes is based on photographs. The flume-averaged bed level defines the reference level. (b) Streamwise evolution of the transverse bed and water surface slopes. (c) Streamwise evolution of the cross-sectional averaged bed and water surface levels.

was fixed by spraying it with paint and the sediment feeding was stopped. Reference is made to *Blanckaert* [2010] for a more detailed account of the bathymetry, the velocity field and the processes causing the velocity redistribution in the M_16_90_00 experiment. Figure 11 shows the steady features of the bathymetry as well as the dune patterns. The most relevant features with respect to inner-bank flow separation are the pronounced point bar and scour pool in the first part of the bend (30° to 105°) as well as just downstream of the bend exit, and the region with a milder transverse bed slope (Figure 11b) in between. As aforementioned, these three distinct regions are representative for zones in natural meander bends of pronounced curvature increase, pronounced curvature decrease and slowly varying curvature, respectively.

[49] The mobile bed topography markedly influences the flow patterns, as illustrated by the pattern of normalized streamwise velocity at the water surface, $v_{s,surface}/U$ in Figure 12. Flow separates from the inner bank over the shallow bars downstream of the bend entry and just

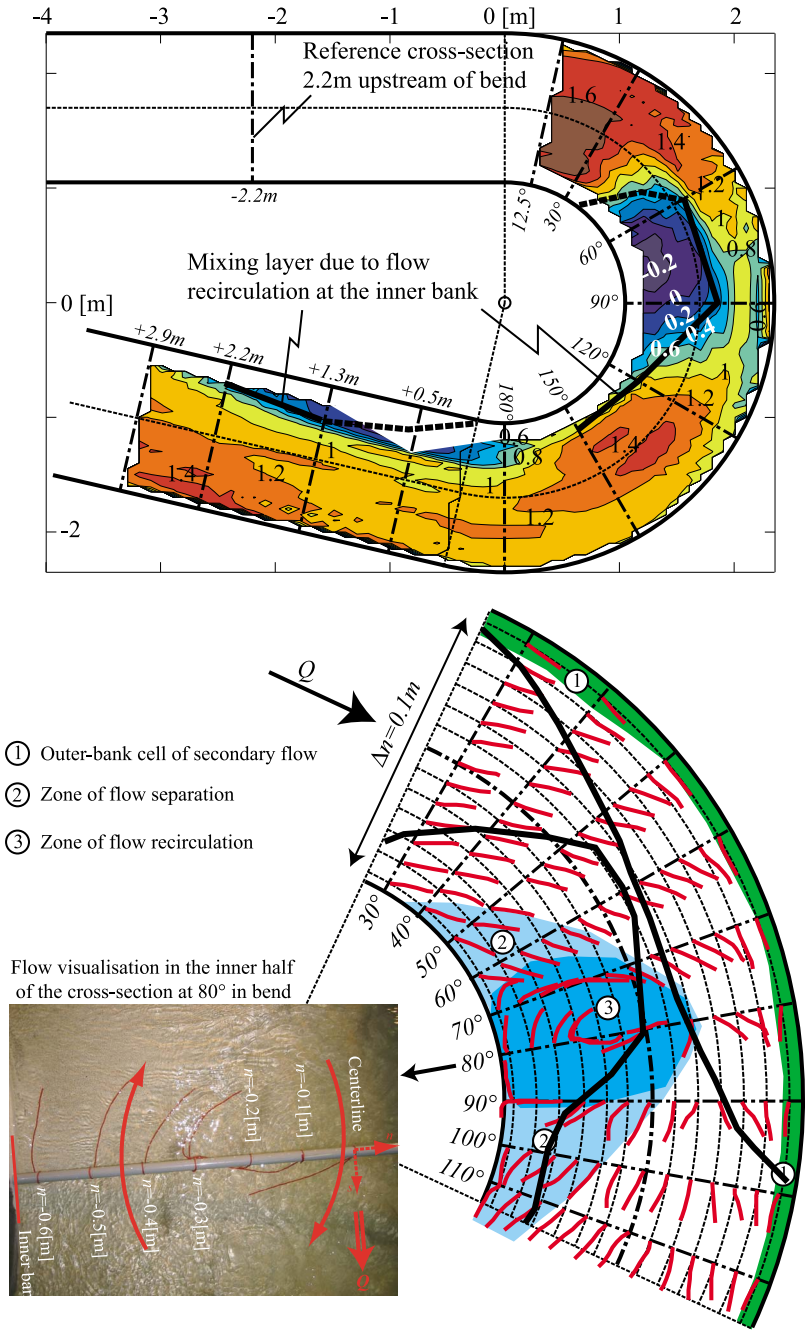

Figure 12. Normalized streamwise velocity at the water surface, v_s/U, in the M_16_90_00 experiment. (top) Isoline pattern based on high-resolution measurements in the indicated cross sections; the experimental uncertainty is estimated as less than 10%. (bottom) Visualization of the flow at the water surface by means of floating wool threads. The black lines delineate approximately the point bar and pool.

downstream of the bend exit (Figures 11 and 12). The shallowness of the flow in both zones of inner-bank flow recirculation did not allow measuring with the ADVP close to the inner bank [*Blanckaert*, 2010]. *van Balen et al.* [2010b] report a detailed description of the flow in both recirculation zones based on calculations with a three-dimensional Large Eddy Simulation code. The flow does not separate from the inner bank at the bend entry but only at about 45° into the bend. This is attributable to the abrupt increase in curvature, which leads to a transverse tilting of the water surface accompanied by pronounced local accelerations/decelerations in the inner/outer half of the cross section and corresponding inward mass transport that opposes flow separation. Visualization by means of wool threads floating on the water surface (picture in Figure 12) allowed identifying a "closed" zone of flow recirculation over the pronounced shallow point bar (Figures 11 and 12), very similar to the sharp natural meander bend modeled by *Ferguson et al.* [2003]. Deposition of

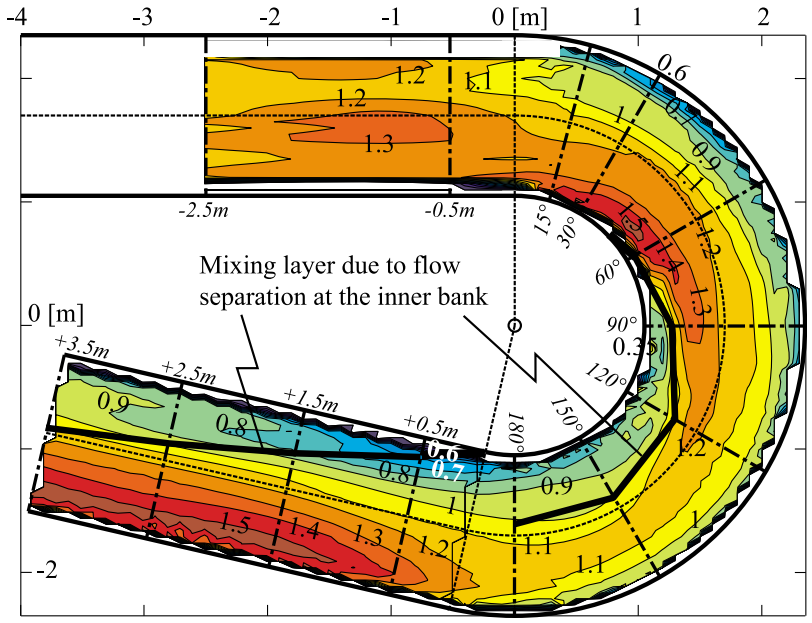

Figure 13. Distribution of the normalized streamwise velocity at the water surface $v_{s,surface}/U$ around the flume in the F_16_90_00 experiment. The edge of the flow separation zone has been determined from the inflexion point in the transverse distribution of $v_{s,surface}$.

sediment in the flow recirculation zone is related to the development of the point bar. The second zone of flow separation just downstream of the bend exit (Figures 11 and 12) is due to the sudden vanishing of the curvature-induced transverse tilting of the water surface, which leads to an adverse pressure gradient at the inner bank, pronounced local decelerations/accelerations in the inner/outer half of the cross section and corresponding outward mass transport. These flow processes promote outer bank erosion. This zone of flow separation, occurring in regions of pronounced curvature decrease, might therefore be relevant with respect to the formation of multilobed meander bends. This hypothesis is in line with observations of a similar zone of inner-bank recirculating flow toward the downstream end of a double-lobed bend by *Frothingham and Rhoads* [2003].

[50] As discussed in section 2, the horizontal bed experiments are not representative of natural meander bends and care should be taken with the extrapolation of results obtained in these experiments toward natural river configuration. Since the M_16_90_00 mobile bed experiment was carried out with the hydraulic parameters of the horizontal-bed F_16_90_00 experiment as initial conditions, comparison of both experiments can provide insight in the role of the interaction between the flow, the sediment transport and the morphology with respect to the inner-bank flow separation.

[51] Similar to the mobile-bed experiment, the flow separates from the inner bank at about 40° in the bend in the horizontal-bed experiment. The region of flow separation is clearly visible in the pattern of the normalized streamwise velocity at the water surface $v_{s,surface}/U$ (Figure 13). Flow separation and the edge of the separation zone have been defined by the occurrence of an internal shear layer, identified based on the classical criterion of the occurrence of an inflexion point in the transverse distribution of the streamwise velocity v_s. The inflexion point was found to coincide with the location of the vertical spiral vortices that indicate the existence of a shear layer (Figure 9). Whereas a "closed" zone of flow recirculation occurred over the pronounced shallow point bar in the bend with mobile bed (Figure 12), a streamwise widening zone of flow separation exists over the horizontal bed (Figure 13). It has a transverse extent of about $4H$ at the bend exit, which is still narrower that the flow recirculation zone in the mobile-bed experiment. The widening of the flow separation zone is accompanied by its weakening: the velocity difference between the flow separation zone and the main flow body and the corresponding inflexion point in the transverse velocity profiles become less pronounced and have almost vanished at the bend exit. Similar to the mobile-bed experiment, a second zone of inner-bank flow separation comes into existence just downstream of the bend exit.

[52] Figure 14 shows the pattern of normalized streamwise velocity, v_s/U, in the F_16_90_00 horizontal bed experiment in the cross section at 90° in the bend, where the center-region cell attains its maximum magnitude. The zone of flow separation has again been defined by the occurrence of an internal shear layer as identified by the occurrence of an inflexion points in the v_s patterns. According to this definition, the flow separation zone is not uniform over the flow depth, but it narrows from the water surface toward the bed and does not even extend over the entire flow depth. The shear layer at the edge of the separation zone is characterized by a sign reversal of the vertical velocities (not shown) and by a core of positive vorticity (Figure 3). This core of positive vorticity does not constitute a counter-rotating secondary flow cell, but rather a zone of opposed vorticity within the center-region cell of secondary flow (a detailed description is reported by K. Blanckaert et al. (Near-bank hydrodynamic processes in open-channel bends and their dependence on the outer-bank roughness, submitted to *Journal of Fluid Mechanics*, 2010)),

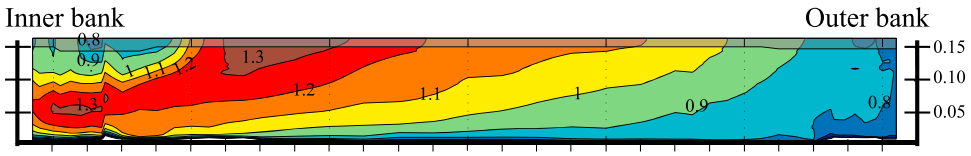

Figure 14. Measured patterns of the normalized streamwise velocity, v_s/U, in the cross section at 90° where the center-region cell of secondary flow attains its maximum amplitude in the F_16_90_00 experiment. The experimental uncertainty is estimated as less than 4%. The image is drawn at an undistorted scale. The flow pattern has been extrapolated in the shaded areas near the water surface where the flow is perturbed by the ADVP housing that touches the water surface.

which stretches onto the inner bank. Figures 3 and 10 indicate the existence of similar hydrodynamic patterns near the inner bank in all horizontal-bed experiments. Figure 15 shows the patterns of the normalized streamwise and transverse velocities, v_s/U (Figure 15, top) and v_n/U (Figure 15, bottom), in the M_16_90_00 mobile-bed experiment. The reported cross section at 90° is situated in the flow recirculation zone over the point bar. Contrary to the horizontal-bed experiment, the curvature-induced center-region cell of secondary flow is isolated over the deepest outer half of the cross section, where it causes the maximum streamwise velocities to occur in the lowest part of the water column.

[53] Comparison of the mobile-bed and horizontal-bed experiments reveals that the interaction between the flow, the sediment transport and the morphology leads to an amplification of the processes and results in fundamentally different hydrodynamic characteristics. The pronounced bar-pool morphology divides the cross section into two distinct regions: a shallow point bar at the inside of the bend and a deep scour pool at the outside of the bend (Figure 11). The

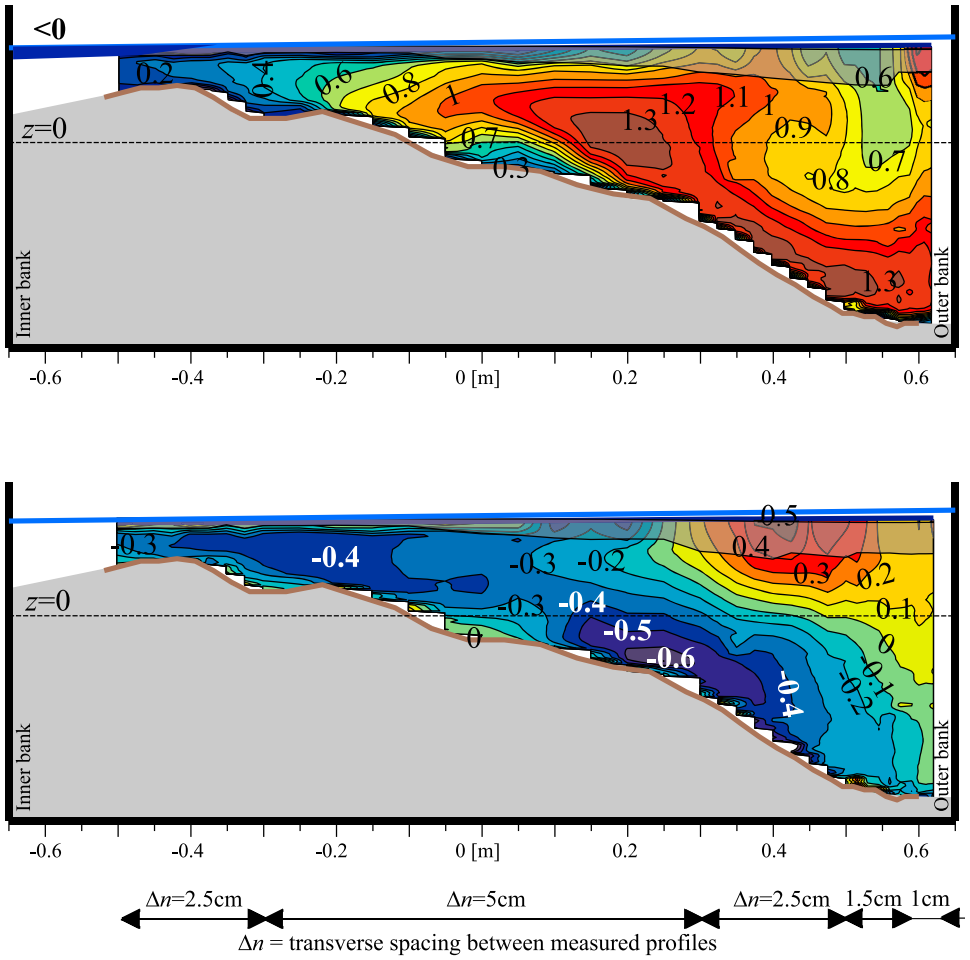

Figure 15. Measured pattern of the normalized streamwise and transverse velocities, (top) v_s/U and (bottom) v_n/U, in the cross section at 90° in the M_16_90_00 experiment. The experimental uncertainty is estimated as less than 4% in v_s and less than 10% in v_n. The images are drawn at undistorted scales. The flow patterns have been extrapolated in the shaded areas near the water surface where the flow is perturbed by the ADVP housing that touches the water surface.

low-velocity recirculating flow on the point bar is efficient in trapping sediment. Moreover, it reduces the effective width considerably and concentrates the overwhelming majority of the discharge in the outer half of the cross section (Figure 12), in agreement with *Bagnold* [1960] and *Leeder and Bridges* [1975]. The increased velocity gradient between the shallow inner part and the deep outer part of the cross section strengthens the free shear layer (Figure 12 versus Figure 13). But the restriction of the width is offset by an increase in cross-sectional area and flow depth in the outer half of the cross section (Figure 11), which leads to a global flow deceleration near the outer bank (Figure 12) in agreement with *Ferguson et al.* [2003]. This deceleration does not necessarily imply that fluid forces are reduced near the outer bank. The three-dimensional flow field (Figure 15) reveals that the streamwise velocity increases near the toe of the outer bank, where the bank is most vulnerable to erosion. Moreover, the increased cross-sectional area is mainly due to important scour near the outer bank (Figures 11 and 15), which promotes bank instability. Overall, these results suggest that inner bank flow separation promotes meander migration and that the bed morphology development enhances the erosive potential near the outer bank.

6. Discussion and Conclusions

[54] When plotted against the curvature ratio B/R, the migration rate of sharp meander bends exhibits large variance, and indicates that some sharply curved bends tend to stabilize (Figure 2). Existing reduced-order numerical models for meander migration are unable to explain and reproduce these observations. The large variance signifies that the single parameter B/R cannot accurately parameterize the complex interplay between numerous hydrodynamic and morphodynamic processes (summarized in Table 1), which may either inhibit or enhance meander migration. These processes and their dependence on hydraulic, geometric and sedimentologic conditions, are still poorly understood and quantified. This paper provided insight in three hydrodynamic processes occurring in sharp meander bends and in the controls that might lead to variations in their relative dominance in different meander bend settings. None of these three hydrodynamic processes is accounted for in existing meander migration models.

[55] Meander migration is largely driven by the curvature-induced secondary flow. Most existing models prescribe the secondary flow to increase linearly with the ratio H/R. Their validity is limited to mild curvatures and slow curvature variations, because they do not account for nonlinear flow interactions that limit the growth of the secondary flow, a process that is called the saturation of the secondary flow. *Blanckaert and de Vriend* [2003, 2010] have developed a nonlinear reduced-order model without restrictions in the curvature and its variation. Their model identifies $C_f^{-1}H/B$ and B/R as the dominant control parameters with respect to meander migration. The former is a characteristic of a river that accounts for the shallowness and the roughness, whereas the latter parameterizes the curvature of individual bends. The influence of the secondary flow saturation generally increases with B/R and $C_f^{-1}H/B$. Although the effect of secondary flow saturation strongly depends on the river planform, the model predicts that it is relevant and inhibits the meander migration rate in moderately and sharply curved bends, $(B/R)_{mean} > 0.33$, on rivers characterized by $C_f^{-1}H/B > 5$ (which is the case in most natural rivers) (Table 2).

[56] Outer bank cells are known to have a protective effect on the (concave) outer bank, which inhibits meander migration. In this study, the outer-bank cells' dependence on bend tightness, bank inclination and bank roughness was investigated in laboratory experiments, which revealed that the magnitude of outer-bank cells shows amplification with increasing bend tightness. As a result, outer-bank cells may be of minor importance with respect to bank erosion in mildly curved meander bends but become relatively more important in very sharply curved meander bends. Outer-bank cells occur over 30° inclined banks, but strengthen and widen when the bank steepens. According to *Leopold and Wolman* [1960] and *Thorne et al.* [1995], the outer bank in natural meander bends steepens with increasing bend tightness, which would further enhance the relative importance of outer-bank cells in tight bends. Outer-bank cells strengthen and widen considerably with increasing roughness of the outer bank, indicating that their protective effect may be more important in natural meander bends with irregular rough banks than in laboratory or numerical experiments.

[57] Comparison of flow separation at the (convex) inner bank in laboratory experiments with a fixed and a mobile bed topography revealed that the interaction between the flow, the sediment transport and the morphology leads to an amplification of the processes and results in fundamentally different characteristics of the flow separation region. Whereas a streamwise widening zone of flow separation exists over the horizontal bed (Figure 13), a "closed" zone of flow recirculation occurs over the pronounced shallow point bar in the bend with mobile bed (Figure 12). This low-velocity recirculating flow is efficient in trapping sediment that builds up the point bar and promotes inner bank accretion. The flow recirculation reduces the effective width considerably and concentrates the discharge and the secondary flow in the outer-half of the cross section (Figure 12), leading to scour near the outer bank and enhanced velocities near the toe of the outer bank (Figures 11 and 15). The control parameters of inner-bank separation remain unknown, but the results suggest that inner-bank flow separation enhances meander migration.

[58] The relative importance of these three hydrodynamic processes in sharp bends strongly depends on hydraulic, geometric and sedimentologic conditions, which is consistent with the different types of meandering proposed by *Hooke* [2003] as well as with the large variance in observed migration rates (Figure 2). The results suggest that secondary flow saturation, which reduces the meander migration rate and promotes meander stabilization, is most relevant in narrow relatively deep rivers ($C_f^{-1}H/B > 10$), whereas large shallow rivers ($C_f^{-1}H/B < 5$) have the most dynamic meandering behavior. Moreover, narrow rivers tend to be characterized by high values of the ratio H/R, which favor the protective effect of the outer-bank cells. Flow separation at the inner bank opposes these tendencies and promotes meander migration, but its dependence on the curvature and the shallowness remains unknown. The correlation with sedimentologic characteristics is expected to further strengthen these tendencies. Highly erodible soils will lead to shallower rivers, less steep banks and a higher migration rate for a given

velocity excess, and therefore to more dynamic meandering behavior.

[59] These qualitative predictions based on a mathematical model and laboratory experiments provide clear testable hypothesis that might help in explaining some of the variance within the observed migration rates presented in Figure 2. Most notably, the results suggest accounting for the influence of the parameter $C_f^{-1}H/B$ in the interpretation and differentiation of the different data sets. The observed variation of the curvature ratio B/R_{max} where the maximum migration rate occurs (Figures 2b–2g), for example, is consistent with the numerical model prediction of the dependence of B/R_{max} on the parameter $C_f^{-1}H/B$ (curve in Figure 6). Unfortunately most field data on meander migration are based on aerial photography and only provide kinematic planform information. They do not provide information on the sediment characteristics, the bathymetry and the flow conditions, which would allow estimating the parameter $C_f^{-1}H/B$. The results and hypothesis of this paper highlight the need for more refined field data.

[60] A quantitative analysis of the role of the three investigated hydrodynamic processes requires their implementation in reduced-order numerical models for meander migration. *Blanckaert and de Vriend*'s [2003, 2010] nonlinear hydrodynamic model, which accounts for secondary flow saturation, can straightforwardly be implemented, as discussed by *Blanckaert and de Vriend* [2010]. The accurate simulation of the outer-bank cells and the inner-bank flow separation requires three-dimensional numerical models. *van Balen et al.* [2010a, 2010b], for example, have successfully simulated both processes in the here reported F_16_90_00 and M_16_90_00 experiments by means of Large Eddy Simulations. Reduced-order models can only account for these processes by means of parameterization, which can be developed according to the following stepwise methodology: (1) a 3-D hydrodynamic model is developed and validated by comparison to the available experimental data; (2) the validated model provides data on important parameters that could not be measured directly, such as the bank shear stress; (3) the validated model allows broadening the investigated parameter space, for example by considering additional values of R/B, C_f, H/B, the inclination and roughness of the banks and other planforms; and (4) the extended data set allows an empirical parameterization of the relevant processes based on the dominant control parameters. *van Balen* [2010] reports progress on steps 1–3 of this combined experimental-numerical methodology with respect to the parameterization of the outer-bank cells.

[61] **Acknowledgments.** This research has been sponsored by the Swiss National Science Foundation under grants 2100-052257, 2000-059392, 2100-066992, 20020-103932, and 200020-119835; by the Deutsche Forschungsgemeinschaft (DFG) and the Netherlands Organization for Scientific Research (NWO) under grants SU 405/3-1 and DN66-149 in the framework of their bilateral cooperation program; and by the Chinese Academy of Sciences fellowship for young international scientists under grant 2009YA1-2. The author acknowledges M. Church, R.I. Ferguson, E.J. Hickin, B.L. Rhoads, S.E. Darby, and three anonymous reviewers for constructive comments that improved the manuscript.

References

Abad, J. D., and M. H. Garcia (2009a), Experiments in a high-amplitude Kinoshita meandering channel: 1. Implications of bend orientation on mean and turbulent flow structure, *Water Resour. Res.*, *45*, W02401, doi:10.1029/2008WR007016.

Abad, J. D., and M. H. Garcia (2009b), Experiments in a high-amplitude Kinoshita meandering channel: 2. Implications of bend orientation on bed morphodynamics, *Water Resour. Res.*, *45*, W02402, doi:10.1029/2008WR007017.

Andrle, R. (1994), Flow structure and development of circular meander pools, *Geomorphology*, *9*, 261–270, doi:10.1016/0169-555X(94)90049-3.

Bagnold, R. A. (1960), Some aspects of the shape of river meanders, *U.S. Geol. Surv. Prof. Pap. 282-E*, U.S. Geol. Surv., Washington, D.C.

Bathurst, J. C., C. R. Thorne, and R. D. Hey (1977), Direct measurements of secondary currents in river bends, *Nature*, *269*, 504–506, doi:10.1038/269504a0.

Bathurst, J. C., C. R. Thorne, and R. D. Hey (1979), Secondary flow and shear stress at river bends, *J. Hydraul. Div. Am. Soc. Civ. Eng.*, *105*(10), 1277–1295.

Begin, Z. B. (1981), Stream curvature and bank erosion: A model based on the momentum equation, *J. Geol.*, *89*, 497–504, doi:10.1086/628610.

Begin, Z. B. (1986), Curvature ratio and rate of river bend migration-update, *J. Hydraul. Eng.*, *112*(10), 904–908, doi:10.1061/(ASCE)0733-9429(1986)112:10(904).

Biedenharn, D. S., P. G. Combs, G. J. Hill, C. F. J. Pinkard, and C. B. Pinkston (1989), Relationship between channel migration and radius of curvature on the Red river, in *Sediment Transport Modeling*, edited by S. S. Y. Wang, pp. 536–541, Am. Soc. Civ. Eng., New York.

Blanckaert, K. (2002), Flow and turbulence in sharp open-channel bends, Ph.D. thesis, number 2545, Ecole Polytech. Fed. Lausanne, Lausanne, Switzerland. (Available at https://documents.epfl.ch/users/b/bl/blanckae/www/Blanckaert_Publications/These_2545_Blanckaert.pdf)

Blanckaert, K. (2009), Saturation of curvature-induced secondary flow, energy losses, and turbulence in sharp open-channel bends: Laboratory experiments, analysis, and modeling, *J. Geophys. Res.*, *114*, F03015, doi:10.1029/2008JF001137.

Blanckaert, K. (2010), Topographic steering, flow recirculation, velocity redistribution and bed topography in sharp meander bends, *Water Resour. Res.*, *46*, W09506, doi:10.1029/2009WR008303.

Blanckaert, K., and H. J. de Vriend (2003), Nonlinear modeling of mean flow redistribution in curved open channels, *Water Resour. Res.*, *39*(12), 1375, doi:10.1029/2003WR002068.

Blanckaert, K., and H. J. de Vriend (2004), Secondary flow in sharp open-channel bends, *J. Fluid Mech.*, *498*, 353–380, doi:10.1017/S0022112003006979.

Blanckaert, K., and H. J. de Vriend (2010), Meander dynamics: A nonlinear model without curvature restrictions for flow in open-channel bends, *J. Geophys. Res.*, *115*, F04011, doi:10.1029/2009JF001301.

Blanckaert, K., and W. H. Graf (2001), Mean flow and turbulence in open-channel bend, *J. Hydraul. Eng.*, *127*(10), 835–847, doi:10.1061/(ASCE)0733-9429(2001)127:10(835).

Blanckaert, K., and W. H. Graf (2004), Momentum transport in sharp open-channel bends, *J. Hydraul. Eng.*, *130*(3), 186–198, doi:10.1061/(ASCE)0733-9429(2004)130:3(186).

Blanckaert, K., and U. Lemmin (2006), Means of noise reduction in acoustic turbulence measurements, *J. Hydraul. Res.*, *44*(1), 3–17, doi:10.1080/00221686.2006.9521657.

Blondeaux, P., and G. Seminara (1985), A unified bar-theory of river meanders, *J. Fluid Mech.*, *157*, 449–470, doi:10.1017/S0022112085002440.

Bolla Pittaluga, M., G. Nobile, and G. Seminara (2009), A nonlinear model for river meandering, *Water Resour. Res.*, *45*, W04432, doi:10.1029/2008WR007298.

Booij, R. (2003), Measurements and large eddy simulations of the flows in some curved flumes, *J. Turbul.*, *4*(8), doi:10.1088/1468-5248/4/1/008.

Bridge, J. S., and J. Jarvis (1977), Velocity profiles and bed shear stress over various bed configurations in a river bend, *Earth Surf. Processes*, *2*, 281–294, doi:10.1002/esp.3290020402.

Camporeale, C., P. Perona, A. Porporato, and L. Rodolfi (2007), Hierarchy of models for meandering rivers and related morphodynamic processes, *Rev. Geophys.*, *45*, RG1001, doi:10.1029/2005RG000185.

Chang, H. H. (1984), Analysis of river meanders, *J. Hydraul. Eng.*, *110*(1), 37–50, doi:10.1061/(ASCE)0733-9429(1984)110:1(37).

Crosato, A. (2008), Analysis and modelling of river meandering, Ph.D. dissertation, Delft Univ. of Technol., Delft, Netherlands.

de Kramer, J., A. Wilbers, J. van den Berg, and M. Kleinhans (2000), De Allier als morfologisch voorbeeld voor de Grensmaas. Deel II: Oevererosie en meandermigratie (in Dutch), *Natuurhist. Maandbl.*, *89*, 189–198.

de Vriend, H. J. (1977), A mathematical model of steady flow in curved shallow channels, *J. Hydraul. Res.*, *15*(1), 37–54, doi:10.1080/00221687709499748.

de Vriend, H. J. (1981), Steady flow in shallow channel bends, *Rep. 81-3*, Lab. Fluid Mech., Dep. Civ. Eng., Delft Univ. Technol., Delft, Netherlands.

de Vriend, H. J., and H. J. Geldof (1983), Main flow velocity in short and sharply curved river bends, *Rep. 83-6*, Lab. Fluid Mech., Dep. Civ. Eng., Delft Univ. Technol. Delft, Netherlands.

Dietrich, W. E., and J. D. Smith (1983), Influence of the point bar on flow through curved channels, *Water Resour. Res.*, *19*, 1173–1192, doi:10.1029/WR019i005p01173.

Duarte, A. (2008), An experimental study on main flow, secondary flow and turbulence in open-channel bends with emphasis on their interaction with the outer-bank geometry, Ph.D. thesis 4227, Ecole Polytech. Fed. Lausanne, Lausanne, Switzerland.

Edwards, B. F., and D. H. Smith (2002), River meandering dynamics, *Phys. Rev. E*, *65*, 046303, doi:10.1103/PhysRevE.65.046303.

Einstein, H. A., and J. A. Harder (1954), Velocity distribution and the boundary layer at channel bends, *Trans. AGU*, *35*(1), 114–120.

Engelund, F. (1974), Flow and bed topography in channel bends, *J. Hydraul. Div. Am. Soc. Civ. Eng.*, *100*(HY11), 1631–1648.

Ferguson, R. I. (1973), Regular meander path models, *Water Resour. Res.*, *9*, 1079–1086, doi:10.1029/WR009i004p01079.

Ferguson, R. I. (1975), Meander irregularity and wavelength estimation, *J. Hydrol.*, *26*(3–4), 315–333, doi:10.1016/0022-1694(75)90012-8.

Ferguson, R. I., D. R. Parsons, S. N. Lane, and R. J. Hardy (2003), Flow in meander bends with recirculation at the inner bank, *Water Resour. Res.*, *39*(11), 1322, doi:10.1029/2003WR001965.

Ferreira da Silva, A. M., and T. El-Tahawy (2008), On the location in flow plan of erosion-deposition zones in sine-generated meandering streams, *J. Hydraul. Res.*, *46*, 49–60.

Ferreira da Silva, A. M., T. El-Tahawy, and W. D. Tape (2006), Variation of flow pattern with sinuosity in sine-generated meandering channels, *J. Hydraul. Eng.*, *132*(10), 1003–1014, doi:10.1061/(ASCE)0733-9429(2006)132:10(1003).

Fong, D. A., S. G. Monismith, M. T. Stacey, and J. R. Burau (2009), Turbulent stresses and secondary currents in a tidal-forced channel with significant curvature and asymmetric bed forms, *J. Hydraul. Eng.*, *135*(3), 198–208, doi:10.1061/(ASCE)0733-9429(2009)135:3(198).

Frothingham, K. M., and B. L. Rhoads (2003), Three-dimensional flow structure and channel change in an asymmetrical compound meander loop, Embarras River, Illinois, *Earth Surf. Processes Landforms*, *28*(6), 625–644, doi:10.1002/esp.471.

Furbish, D. J. (1988), River-bend curvature and migration: How are they related?, *Geology*, *16*(8), 752–755, doi:10.1130/0091-7613(1988)016<0752:RBCAMH>2.3.CO;2.

Güneralp, I., and B. L. Rhoads (2009), Empirical analysis of the planform curvature-migration relation of meandering rivers, *Water Resour. Res.*, *45*, W09424, doi:10.1029/2008WR007533.

Güneralp, I., and B. L. Rhoads (2010), The spatial autoregressive structure of meander evolution revisited, *Geomorphology*, *120*, 90–106, doi:10.1016/j.geomorph.2010.02.010.

Hey, R. D., and C. R. Thorne (1975), Secondary flow in river channels, *Area*, *7*(3), 191–195.

Hickin, E. J. (1974), The development of meanders in natural river-channels, *Am. J. Sci.*, *274*, 414–442, doi:10.2475/ajs.274.4.414.

Hickin, E. J. (1977), Hydraulic factors controlling channel migration, in *Research in Fluvial Geomorphology: Proceedings of the 5th Guelph Geomorphology Symposium*, edited by R. E. Davidson-Arnott and W. Nickling, pp. 59–66, Geobooks, Norwich, U. K.

Hickin, E. J. (1978), Mean flow-structure in meanders of the Squamish River, British Columbia, *Can. J. Earth Sci.*, *15*(11), 1833–1849.

Hickin, E. J., and G. C. Nanson (1975), The character of channel migration on the Beatton river, northeast British Columbia, Canada, *Geol. Soc. Am. Bull.*, *86*, 487–494, doi:10.1130/0016-7606(1975)86<487:TCOCMO>2.0.CO;2.

Hickin, E. J., and G. C. Nanson (1984), Lateral migration rates of river bends, *J. Hydraul. Eng.*, *110*(11), 1557–1567, doi:10.1061/(ASCE)0733-9429(1984)110:11(1557).

Hodskinson, A., and R. I. Ferguson (1998), Numerical modelling of separated flow in river bends: Model testing and experimental investigation of geometric controls on the extent of flow separation at the concave bank, *Hydrol. Processes*, *12*, 1323–1338, doi:10.1002/(SICI)1099-1085(19980630)12:8<1323::AID-HYP617>3.0.CO;2-S.

Hooke, J. M. (1987), Changes in meander morphology, in *International Geomorphology, 1986: Proceedings of the First International Conference on Geomorphology*, vol. 1, edited by V. Gardiner, pp. 591–609, Wiley, Chichester, U. K.

Hooke, J. (2003), River meander behaviour and instability: A framework for analyses, *Trans. Inst. Br. Geogr.*, *28*(2), 238–253, doi:10.1111/1475-5661.00089.

Howard, A. D. (1984), Simulation model of meandering, in *River Meandering*, edited by C. M. Elliott, pp. 952–963, Am. Soc. of Civ. Eng., Reston, Va.

Hudson, P. F., and R. H. Kesel (2000), Channel migration and meander-bend curvature in the lower Mississippi River prior to major human modification, *Geology*, *28*(6), 531–534, doi:10.1130/0091-7613(2000)28<531:CMAMCI>2.0.CO;2.

Hurther, D. (2001), 3-D acoustic Doppler velocimetry and turbulence in open-channel flow, Ph.D. thesis 2395, Ecole Polytech. Fed. Lausanne, Lausanne, Switzerland.

Ikeda, S., G. Parker, and K. Sawai (1981), Bend theory of river meanders. Part 1. Linear development, *J. Fluid Mech.*, *112*, 363–377, doi:10.1017/S0022112081000451.

Imran, J., G. Parker, and C. Pirmez (1999), A nonlinear model of flow in meandering submarine and subaerial channels, *J. Fluid Mech.*, *400*, 295–331, doi:10.1017/S0022112099006515.

Jackson, A. D. (1992), Bedload transport and sorting in meander bends, Fall River, Rocky Mountain National Park, Colorado, Ph.D. thesis, 280 pp., Colo. State Univ., Fort Collins.

Jia, Y., and S. S. Y. Wang (2000), Numerical simulation of the channel flow with submerged weirs in Victoria Bendway, Mississippi River, Tech. Rep. NCCHE-TR-2000-3, U.S. Army Corps of Eng. Res. and Dev. Cent., Vicksburg, Miss.

Johannesson, H., and G. Parker (1989a), Velocity redistribution in meandering rivers, *J. Hydraul. Eng.*, *115*(8), 1019–1039, doi:10.1061/(ASCE)0733-9429(1989)115:8(1019).

Johannesson, H., and G. Parker (1989b), Linear theory of river meanders, in *River Meandering*, *Water Resour. Monogr.*, vol. 12, edited by S. Ikeda and G. Parker, pp. 181–213, AGU, Washington, D. C.

Julien, P. Y., G. J. Klaassen, W. B. M. Ten Brinke, and W. E. Wilber (2002), Case study: Bed resistance of Rhine River during 1998 flood, *J. Hydraul. Eng.*, *128*(12), 1042–1050, doi:10.1061/(ASCE)0733-9429(2002)128:12(1042).

Lancaster, S. T., and R. L. Bras (2002), A simple model of river meandering and its comparison to natural channels, *Hydrol. Processes*, *16*, 1–26, doi:10.1002/hyp.273.

Leeder, M. R., and P. H. Bridges (1975), Flow separation in meander bends, *Nature*, *253*(5490), 338–339, doi:10.1038/253338a0.

Leopold, L. B., and M. G. Wolman (1960), River meanders, *Geol. Soc. Am. Bull.*, *71*, 769–794, doi:10.1130/0016-7606(1960)71[769:RM]2.0.CO;2.

Liverpool, T. B., and S. F. Edwards (1995), Dynamics of a meandering river, *Phys. Rev. Lett.*, *75*(16), 3016–3019, doi:10.1103/PhysRevLett.75.3016.

Markham, A. J., and C. R. Thorne (1992), Geomorphology of gravel-bed river bends, in *Dynamics of Gravel-Bed Rivers*, edited by P. Billi et al., pp. 433–456, Wiley, Chichester, U. K.

Mockmore, C. A. (1943), Flow around bends in stable channels, *Trans. Am. Soc. Civ. Eng.*, *109*, 593–628.

Nanson, R. A. (2010), Flow fields in tightly curving meander bends of low width-depth ratio, *Earth Surf. Processes Landforms*, *35*(2), 119–135.

Nanson, G. C., and E. J. Hickin (1983), Channel migration and incision on the Beatton river, *J. Hydraul. Eng.*, *109*(3), 327–337, doi:10.1061/(ASCE)0733-9429(1983)109:3(327).

Nanson, G. C., and E. J. Hickin (1986), A statistical analysis of bank erosion and channel migration in western Canada, *Geol. Soc. Am. Bull.*, *97*, 497–504, doi:10.1130/0016-7606(1986)97<497:ASAOBE>2.0.CO;2.

Odgaard, A. J. (1981), Transverse bed slope in alluvial channel bends, *J. Hydraul. Div. Am. Soc. Civ. Eng.*, *107*(HY12), 1677–1693.

Odgaard, A. J. (1984), Bank erosion contribution to stream sediment load, *IIHR Rep. 280*, Iowa Inst. of Hydraul. Res., Univ. of Iowa, Iowa City.

Odgaard, A. J. (1986), Meander flow model. I: Development, *J. Hydraul. Eng.*, *112*(12), 1117–1136, doi:10.1061/(ASCE)0733-9429(1986)112:12(1117).

Odgaard, A. J. (1989), River-meander model. I: Development, *J. Hydraul. Eng.*, *115*(11), 1433–1450, doi:10.1061/(ASCE)0733-9429(1989)115:11(1433).

Odgaard, A. J., and M. A. Bergs (1988), Flow processes in a curved alluvial channel, *Water Resour. Res.*, *24*, 45–56, doi:10.1029/WR024i001p00045.

Olesen, K. W. (1987), Bed topography in shallow river bends, Ph.D. thesis, Delft Univ. of Technol., Delft, Netherlands.

Parker, G., and E. D. Andrews (1986), On the time development of meander bends, *J. Fluid Mech.*, *162*, 139–156, doi:10.1017/S0022112086001970.

Parker, G., K. Sawai, and S. Ikeda (1982), Bend theory of river meanders. Part 2. Nonlinear deformation of finite-amplitude bends, *J. Fluid Mech.*, *115*, 303–314, doi:10.1017/S0022112082000767.

Parker, G., P. Diplas, and J. Akiyama (1983), Meander bends of high amplitude, *J. Hydraul. Eng.*, *109*(10), 1323–1337, doi:10.1061/(ASCE)0733-9429(1983)109:10(1323).

Pizzuto, J., and T. Meckelnburg (1989), Evaluation of a linear bank erosion equation, *Water Resour. Res.*, *25*, 1005–1013, doi:10.1029/WR025i005p01005.

Post, G., and C. D. Rennie (2007), The distribution of Reynolds stresses in a model channel bend measured using ADVs, in *Proceedings of 2007 Hydraulic Measurements and Experimental Methods Conference: Lake Placid, NY*, edited by E. A. Cowin, pp. 332–338, Am. Soc. Civ. Eng., Reston, Va.

Rhoads, B. L., and K. D. Massey (2010), Flow structure and channel change in a sinuous grass-lined stream within an agricultural drainage ditch: Implications for ditch stability and aquatic habitat, *River Res. Appl.*, doi:10.1002/rra.1430, in press.

Roca, M., K. Blanckaert, and J. P. Martin-Vide (2009), Reduction of bend scour by an outer bank footing: flow field and turbulence, *J. Hydraul. Eng.*, *135*(5), 361–368, doi:10.1061/(ASCE)HY.1943-7900.0000028.

Rozovskii, I. L. (1957), *Flow of Water in Bends of Open Channels* (in Russian), Acad. of Sci. of the Ukranian SSR, Kiev. (English translation, Isr. Program for Sci. Transl., Jerusalem, 1961.)

Seminara, G. (2006), Meanders, *J. Fluid Mech.*, *554*, 271–297, doi:10.1017/S0022112006008925.

Seminara, G., and M. Tubino (1992), Weakly nonlinear theory of regular meanders, *J. Fluid Mech.*, *244*, 257–288, doi:10.1017/S0022112092003069.

Seminara, G., G. Zolezziu, M. Tubino, and D. Zardi (2001), Downstream and upstream influence in river meandering. Part 2. Planimetric development, *J. Fluid Mech.*, *438*, 213–230, doi:10.1017/S0022112001004281.

Stølum, H.-H. (1996), River meandering as a self-organization process, *Science*, *271*, 1710–1713, doi:10.1126/science.271.5256.1710.

Stølum, H.-H. (1998), Planform geometry and dynamics of meandering rivers, *Geol. Soc. Am. Bull.*, *110*(11), 1485–1498, doi:10.1130/0016-7606(1998)110<1485:PGADOM>2.3.CO;2.

Sun, T., P. Meakin, T. Jøssang, and K. Schwarz (1996), A simulation model for meandering rivers, *Water Resour. Res.*, *32*, 2937–2954, doi:10.1029/96WR00998.

Thorne, C. R., and R. D. Hey (1979), Direct measurements of secondary currents at a river inflexion point, *Nature*, *280*, 226–228, doi:10.1038/280226a0.

Thorne, C. R., L. W. Zevenbergen, J. C. Pitlick, S. Rais, J. B. Bradley, and P. Y. Julien (1985), Direct measurement of secondary currents in a meandering sand-bed river, *Nature*, *315*, 746–747, doi:10.1038/315746a0.

Thorne, C. R., S. R. Abt, and S. T. Maynord (1995), Prediction of near-bank velocity and scour depth in meander bends for design of riprap revetments, in *River, Coastal and Shoreline Protection: Erosion Control Using Riprap and Armourstone*, edited by C. R. Thorne et al., pp. 115–133, Wiley, Chichester, U. K.

van Balen, W. (2010), Large eddy flow simulation for the prediction of bank erosion and transport processes in river bends, Ph.D. dissertation, Delft Univ. of Technol., Delft, Netherlands.

van Balen, W., K. Blanckaert, and W. S. J. Uijttewaal (2010a), Analysis of the role of turbulence in curved open-channel flow at different water depths by means of experiments, LES and RANS, *J. Turbul.*, *11*, doi:10.1080/14685241003789404.

van Balen, W., W. S. J. Uijttewaal, and K. Blanckaert (2010b), Large-eddy simulation of a curved open-channel flow over topography, *Phys. Fluids*, *22*, 075108, doi:10.1063/1.3459152.

van Bendegom, L. (1947), Eenige beschouwingen over riviermorphologie en rivierverbetering (in Dutch), *De Ingenieur*, *59*(4), 1–11.

van Rijn, L. C. (1984), Sediment transport, Part III: Bed forms and alluvial roughness, *J. Hydraul. Eng.*, *110*(12), 1733–1754, doi:10.1061/(ASCE)0733-9429(1984)110:12(1733).

Whiting, P. J., and W. E. Dietrich (1993), Experimental studies of bed topography and flow patterns in large-amplitude meanders: 1. Observations, *Water Resour. Res.*, *29*, 3605–3614, doi:10.1029/93WR01755.

Yeh, K. C., and J. F. Kennedy (1993), Moment model of nonuniform channel-bend flow. I. Fixed beds, *J. Hydraul. Eng.*, *119*(7), 776–795, doi:10.1061/(ASCE)0733-9429(1993)119:7(776).

Zimmerman, C., and J. F. Kennedy (1978), Transverse bed slopes in curved alluvial channels, *J. Hydraul. Eng.*, *104*, 33–48.

Zolezzi, G., and G. Seminara (2001), Downstream and upstream influence in river meandering. Part 1. General theory and application to overdeepening, *J. Fluid Mech.*, *438*, 183–211.

K. Blanckaert, Laboratory of Hydraulic Constructions, School of Architecture, Civil and Environment Engineering, École Polytechnique Fédérale Lausanne, CH-1015 Lausanne, Switzerland. (koen.blanckaert@epfl.ch)